

Water-in-Salt Electrolyte (WiSE) for Aqueous Batteries: A Long Way to Practicality

Léa Droguet, Alexis Grimaud, Olivier Fontaine, Jean-marie Tarascon

▶ **To cite this version:**

Léa Droguet, Alexis Grimaud, Olivier Fontaine, Jean-marie Tarascon. Water-in-Salt Electrolyte (WiSE) for Aqueous Batteries: A Long Way to Practicality. Advanced Energy Materials, 2020, pp.2002440. 10.1002/aenm.202002440 . hal-03000052

HAL Id: hal-03000052
https://hal.science/hal-03000052

Submitted on 11 Nov 2020

HAL is a multi-disciplinary open access archive for the deposit and dissemination of scientific research documents, whether they are published or not. The documents may come from teaching and research institutions in France or abroad, or from public or private research centers.

L'archive ouverte pluridisciplinaire **HAL**, est destinée au dépôt et à la diffusion de documents scientifiques de niveau recherche, publiés ou non, émanant des établissements d'enseignement et de recherche français ou étrangers, des laboratoires publics ou privés.

Water-in-salt Electrolyte (WiSE) for Aqueous Batteries:

A Long Way to Practicality

Léa Droguet [a],[b],[c], Alexis Grimaud [a],[c], Olivier Fontaine [c],[d], Jean-Marie Tarascon [a],[b],[c]**

[a] Chimie du Solide et de l'Energie, UMR 8260, Collège de France, 11 place Marcelin Berthelot, 75231 Paris Cedex 05, France

[b] Sorbonne Université, 4 place Jussieu, 75005 Paris, France

[c] Réseau sur le stockage Electrochimique de l'Energie (RS2E), CNRS FR3459, 33 rue Saint Leu, 80039 Amiens Cedex, France

[d] Institut Charles Gerhardt Montpellier, Université Montpellier, UMR 5253, Place Eugène Bataillon, 34095 Montpellier, France

* Corresponding authors

Alexis Grimaud: alexis.grimaud@college-de-france.fr

Jean-Marie Tarascon : jean-marie.tarascon@college-de-france.fr

Keywords : aqueous batteries, water-in-salt, figure of merit, self-discharge, SEI stability, superconcentrated electrolyte, lithium ion

Abstract

Sustainability of battery component is becoming an overriding parameter for storing renewable energy at large scale. Toward that goal, several strategies are currently being explored. Great hopes are being placed in the use of superconcentrated aqueous electrolytes, which enlarge the electrochemical stability window well beyond 1.2 V. Although fundamentally elegant, the practicability of such approach remains unknown. Therefore, we perform an in-depth analysis of the stability and cycling behavior of *Water-in-salt* (WiSE) and *Water-in-bisalt* (WiBS) *(LiTFSI-LiBETI)* electrolytes as a function of concentration and temperature at both electrodes by monitoring via combined o*perando* gas monitoring, cyclic voltammetry, and self-discharge experiments the SEI growth and stability. The SEI formed on the negative electrode is found inefficient in protecting the battery against continuous electrolyte degradation through water reduction during both cycling and storage; this inefficiency being increased at elevated temperatures. This result contrasts with the impact of water oxidation that is less severe. We benchmark our data against other commercial batteries. We show that WiSE-based battery in their current form cannot compete with Lead-acid, Ni-Cd or Ni-MH commercial aqueous batteries in terms of price, operating temperature range, lifetime, and capacity fading upon storage. So the practical outcome of the superconcentrated aqueous electrolyte remains highly uncertain.

1. Introduction

Li-ion batteries, because of their outstanding performances, have become an integral part of our society. However, a remaining challenge regards ways to lower their cost and improve their sustainability. Toward that ambitious goal, several strategies are currently being explored, one being the use of aqueous electrolytes that are theoretically cheaper, safer, and less toxic than their organic counterparts. However, the major limitation in the development of aqueous electrolytes is the narrow thermodynamic electrochemical stability window (ESW) of water (1.23 V). Although it can be kinetically extended to 1.5 V when using salts in a diluted solution, such aqueous systems still do not compete against organic ones. Owing to this limitation that translates into poor energy density, Li-aqueous systems, as introduced in 1994 by Dahn and coworkers, could never be marketed.[1]

To alleviate this issue, in continuation of early works dedicated to the development of superconcentrated organic electrolytes,[2] Suo *et al.*[3] proposed in 2015, an aqueous electrolyte made with a high salt concentration (21 mol kg^{-1}: 21 m), denoted *Water-in-salt electrolytes* (WiSE). Through this trick, the authors could enlarge the operating potential window of aqueous systems to 3 V while preserving an ionic conductivity alike that of classical organic electrolytes (ar. 10 mS cm^{-1}). As a proof of concept, a 2.3 V battery using Mo_6S_8 and $LiMn_2O_4$ as negative and positive electrodes, respectively, was reported. Following this demonstration, Yamada *et al.*[4] then showed that mixing two organic lithium salts, thus forming a so-called *Water-in-bisalt electrolyte* (WiBS), enables assembling aqueous batteries with a working potential as high as 3.1 V using $Li_4Ti_5O_{12}$ and $LiNi_{0.5}Mn_{1.5}O_4$ electrodes. Altogether, these studies have renewed interest for revisiting aqueous systems relying on the use of superconcentrated electrolytes, hence the recent reports on aqueous Na-ion,[5]–[9] K-ion,[10]–[13] Li-O_2[14] or even quasi-solid-state batteries based on, *e.g.,* polymer hydrogel electrolytes.[15]–[19]

Different types of superconcentrated aqueous electrolytes are currently investigated for Li-aqueous systems. Most frequently used is the *Water-in-salt* electrolyte based on one lithium salt,[3][20][21] usually LiTFSI or TFSI-derived salts which have the specificity to form F-based solid electrolyte interphase (SEI) at high concentrations.[22][23] Superconcentrated electrolytes using either two lithium-based salts,[4][24]–[26] or one Li-based salt and one non-Li-based one, [27][28] referred as *Water-in-bisalt* (WiBS) electrolytes, are also getting some momentum. Whatever Li-based or Li-free salts, asymmetric ions are preferred as they increase the solubility of the Li-based salt, hence enabling to design electrolytes with greater salt concentration. The benefits of both WiSEs and WiBSs electrolytes systems are rooted in their ability to form an SEI while lowering the amount of free water molecules, hence minimizing chances of SEI dissolution in the bulk electrolyte.[29]

The origin for the enlarged electrochemical window offered by such electrolytes has been described by the occurrence of specific physical-chemical interactions at the negative and positive electrodes. At the negative electrode, the high salt concentration modifies the solvation sheath of lithium cations as well as of the anions, thus enabling the electrochemical formation of an SEI.[3] The exact mechanism for the SEI formation is still under debate, but its insulating nature was claimed to prevent further water reduction (hydrogen evolution reaction: HER) from happening.[20][30] Turning to the positive electrode, the negatively charged solvated anion species move first towards the electrode to form an hydrophobic organic anion-rich double layer that repeals water molecules, thus preventing their oxidation (oxygen evolution reaction: OER).[22][31][32] In conclusion, the formation of, both, a stable SEI and a hydrophobic double layer were brought to explain the widening of the ESW.

Besides, the ESW widening was previously assessed using metallic current collectors such as platinum, conductive glassy carbon or directly with current collectors materials (titanium, stainless steel or aluminum) with overpotential greater than 500 mV measured for the OER[4][5][28][32]–[34]

using superconcentrated electrolytes. Instead, almost no change is observed for the HER overpotential as a function of the metallic current collector [32][33] when increasing the salt concentration, the exception being aluminum that passivates.[4][29][34]–[36] However, we must exercise caution in hastily interpreting these potential shifts that are determined by cyclic voltammetry measurements rather than by potentio/galvano-static methods, hence departing from practical conditions. Indeed, by narrowing down the number of testing parameters, especially when the threshold current density is not taking into account, the influence of parasitic reactions such as the HER can be downplayed, as recently discussed by Kühnel *et al.*[35] Therefore, despite the blooming number of superconcentrated aqueous electrolytes developed in the past few years, the viability of such systems in real conditions remains uncertain. Thus, we decided to embark on an in-depth study to assess the viability of batteries based on either 20 m LiTFSI WiSE or 20 m LiTFSI: 8 m LiBETI WiBS by first focusing on a full understanding of the parasitic reactions occurring on both the cathodic and the anodic side. This enlists electrochemical tests to estimate cell performances upon varying concentrations and temperatures. Equally, the role of parasitic reactions on battery performances was studied by o*perando* gas monitoring, while cyclic voltammetry and self-discharge experiments enabled us to assess the SEI stability over time. Lastly, we provide the figure of merits for WiSEs-based aqueous Li-ion batteries and compare this technology with existing aqueous technologies (Pb-acid, Ni-Cd, Ni-MH) and aprotic Li-ion batteries.

2. Results

2.1 Definition of the practical conditions

Prior to the study of the effect of C-rate, temperature, and self-discharge on the performances of WiSEs-based aqueous batteries, proper current collectors, as well as counter and working electrode materials, must be selected. **Figure 1a and Figure S 1** shows the ESW of titanium and stainless steel plungers used for the positive and negative electrode, respectively. A titanium

current collector was selected for positive electrode since it allows cycling $LiNi_{0.6}Mn_{0.2}Co_{0.2}O_2$ (NMC_{622}) without any sign of OER activity. In contrast, stainless steel current collectors can be used as positive or negative electrodes for the insertion/de-insertion potential of Mo_6S_8, $LiFePO_4$ (LFP) and $LiTi_2(PO_4)_3$ (LTP) electrode materials since neither water oxidation nor reduction occurs over their range of electrochemical activity [37]–[39]. To independently assess the parasitic reactions occurring at the negative electrode from those at the positive electrode, LFP was chosen as counter electrode for testing Mo_6S_8 negative electrode. In contrast, LTP was selected for testing NMC_{622} as positive electrode. Indeed, using a 3-electrodes Swagelok cell with an Ag/AgCl reference electrode, both LFP, and LTP counter electrodes, known to reversibly exchange Li^+ in aqueous electrolytes,[37]–[39] were found to have their redox potential within the ESW of the WiSEs electrolyte studied in this work (Figure 1a).

Having defined the proper current collectors and active materials, full cells were thus assembled to study the effect of WiSEs on the redox properties of both active materials, Mo_6S_8 and NMC_{622}, measured against LFP and LTP, respectively (**Figure 1b**). After checking the redox potentials for LFP and LTP versus the potential of Ag/AgCl reference electrode, the potentials for the working electrodes were rescaled versus Li^+/Li. Doing so, an upshift in open-circuit voltage of ≈ 230 mV is observed when cycling Mo_6S_8 and NMC_{622} in WiSE compared to the organic electrolyte (1 M $LiPF_6$ in EC:DMC, *e.g.* LP30). This shift, previously observed when using more classical reference electrodes, was assigned to the effect of the salt concentration on the redox potential of the intercalation electrodes.[4] Such an upshift of the intercalation potential combined with the use of cutoff potential of 4.2 V defined *vs.* Li^+/Li in charge explains the lower measured capacity of NMC_{622} in WiSE as opposed to non-aqueous electrolytes. The importance of adequately selecting this cutoff potential will be discussed in greater detail.

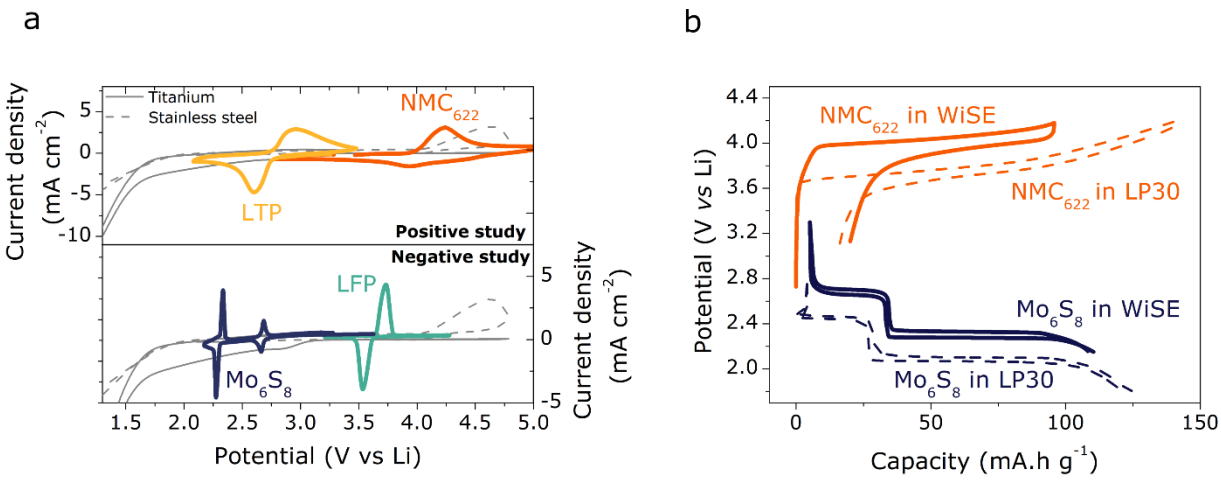


Figure 1. (a) Electrochemical stability window of current collectors and reversibility of Li^+ intercalation/de-intercalation of electrode materials in 20 m LiTFSI. Cyclic voltammograms performed at 100 mV s^{-1} on stainless steel (grey dash line) or Titanium (grey full line) as working electrode (WE), Pt wire as counter electrode (CE) and Ag/AgCl as reference. Cyclic voltammograms performed at 1 mV s^{-1} on Mo_6S_8 (dark blue), LFP (light blue), LTP (yellow) NMC_{622} (orange) as WE, YP50 activated carbon as CE and Ag/AgCl as reference electrode. (b) Galvanostatic charge and discharge signatures for electrode materials. Galvanostatic experiment performed at 1C on Mo_6S_8 measured in LP30 versus Li metal and 20 m LiTFSI versus LFP on SS current collector (1st cycle). Galvanostatic experiment performed at 0.10C on $LiNi_{0.6}Mn_{0.2}Co_{0.2}O_2$ measured in LP30 versus Li metal and 20 m LiTFSI versus LTP on Ti current collector (1st cycle). All experiments were performed at room temperature.

2.2 Use of *Water-in-salt* electrolyte: effect on the negative electrode

2.2.1. Effect of electrolyte concentration on the Mo_6S_8/LFP system

The capacities in charge and discharge of a Mo_6S_8/LFP cell were measured as a function of the salt concentration from 5 m up to 20 m, corresponding to *Water-in-salt* electrolyte. Cell capacity and Coulombic efficiency measured at 1C at room temperature are shown in **Figure 2a** and **2b**. There, the difference between charge and discharge capacities is becoming greater when lowering the salt concentration, *i.e.,* the Coulombic efficiency is decreasing. Furthermore, the capacity is found to fade over cycling much faster when lowering the salt concentration. These results can tentatively be interpreted either as the sign that no SEI is formed at lower concentrations or by invoking a higher solubility of inorganic compounds forming the SEI, such as LiF,[20][30] Li_2O[20] or LiOH[30] previously observed forming on the surface of negative electrodes, at lower

concentrations. Either way, the continuous parasitic reactions occurring on the surface of Mo_6S_8 negative electrode consume Li^+ and cause the performances to decay over cycling at low concentration. Finally, and more interestingly, the initial capacity in charge is found in Figure 2a, similar to the different concentrations: 125 mA.h g^{-1} at 5 m, 120 mA.h g^{-1} at 10 m and 123 mA.h g^{-1} at 20 m, suggesting that the nature and the number of parasitic reactions are independent of the concentration during the first charge, before the formation of an SEI.

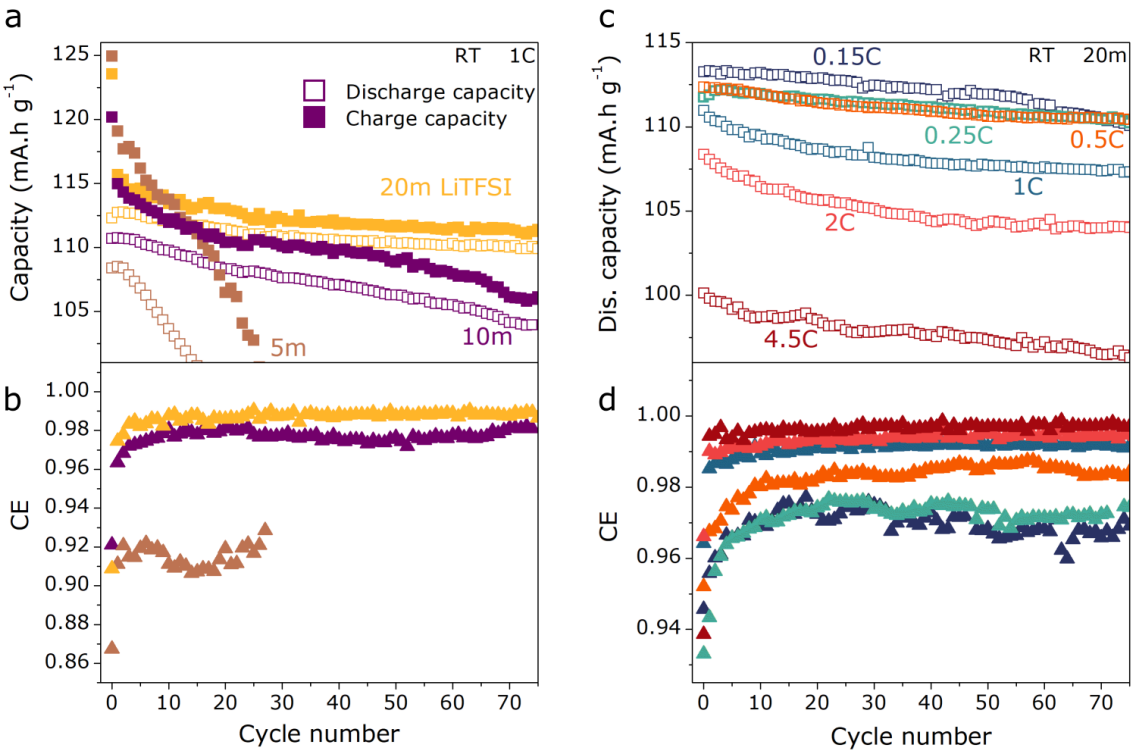


Figure 2. Effect of concentration and C-rate on Mo_6S_8/$LiFePO_4$ full cell in LiTFSI-based aqueous electrolytes. (a) Capacities of charge and discharge and (b) Coulombic efficiency (CE) as a function of cycle number for several concentrations: 5 m LiTFSI (brown square), 10 m LiTFSI (purple square), 20 m LiTFSI (yellow square). Constant current measurements were performed at 1C at room temperature. (c) Capacity of discharge (Dis. Capacity) and (d) Coulombic efficiency as function of cycle number for several C-rate: 0.15C, 0.25C, 0.5C, 1C, 2C, 4.5C. Constant current measurements were performed in 20 m LiTFSI electrolyte at room temperature.

2.2.2 Influence of the cycling rate on the Mo_6S_8/LFP system

Even though the cycling performances improve with concentration, they are dependent on the cycling rate, as shown in **Figure 2c** and **2d** where the evolution of the discharge capacity (Figure 2c) and the Coulombic efficiency (Figure 2d) are reported for several C-rates at room temperature. Indeed, it clearly appears that the faster the cycling rate is, the higher the Coulombic efficiency (Figure 2d). However, the absolute value for the capacity is slightly lower (Figure 2c), hence leading to significant improvements in the cell capacity retention. This phenomenon can be related to greater amount of parasitic reactions occurring as time spent at potential close to the HER reversible potential increases when lowering the C-rate, thus artificially increasing the charge capacity at the expense of the discharge capacity. As a result, and as often seen in the literature,[35] one obvious way to increase the Coulombic efficiency and cycling performances of such systems is by increasing the C-rate. However, our work reveals that C-rate below 1C must be employed to accurately evaluate the performances of aqueous systems in this configuration.

2.2.3 Origin of the performances decay: gas monitoring

We then performed operando gas monitoring using a combination of online electrochemical mass spectrometry (OEMS) and pressure cells to qualitatively and quantitatively interrogate the impact of gas evolution on the battery performances. **Figure 3a** shows the potential and pressure changes as a function of time during cycling for 20 m LiTFSI electrolyte. There, the cell pressure is found to increase when the potential reaches the 2nd lithium insertion plateau of Mo_6S_8 (≈ 1.4 V in a complete Mo_6S_8/LFP cell, see **Figure 3b** for the definition of the plateau). Strikingly, the pressure never stops increasing in this configuration during cycling, demonstrating that parasitic reactions keep occurring, consistent with the low Coulombic efficiency observed in Figure 2d. Moreover, from OEMS measurements (Figure 3b), we could deduce the formation of gaseous hydrogen as

soon as Mo_6S_8 reaches its second lithium insertion plateau. Therefore, water reduction producing hydrogen is responsible for the pressure increase, and any SEI formed on the electrode at these potentials is not protective enough to prevent the continuous consumption of WiSE during cycling. Besides, it is important to notice that hydrogen evolution competes with lithium insertion, but the former does not prevent the latter. Hence, two rates for the electrochemical hydrogen evolution were observed in **Figure 3**b. The first rate starts concomitantly with the 2^{nd} insertion of lithium around 1.38V. However, this first rate is slow compared to the one kicking in once the electrode is fully lithiated, when the potential goes above 1.4 V and where all electrons are consumed toward the HER. Moreover, as seen in **Table S 1** (see Supporting information) the discharge capacity recorded with a pressure cell cycled at 0.10C remains stable at *ar.* 107.5 mA.h g^{-1} during the 4 first cycles, unlike the charge capacity which is always greater and varies from 126 to 117 mAh g^{-1}. This result indicates that lithium insertion into Mo_6S_8 is not affected by the HER during charge, as the cell provides the same discharge capacity over the first cycles. However, the continuous consumption of water *via* the HER may eventually lead to the crystallization of the salt and ultimately the drying out of the cell, that will be prejudicial for practical application [35].

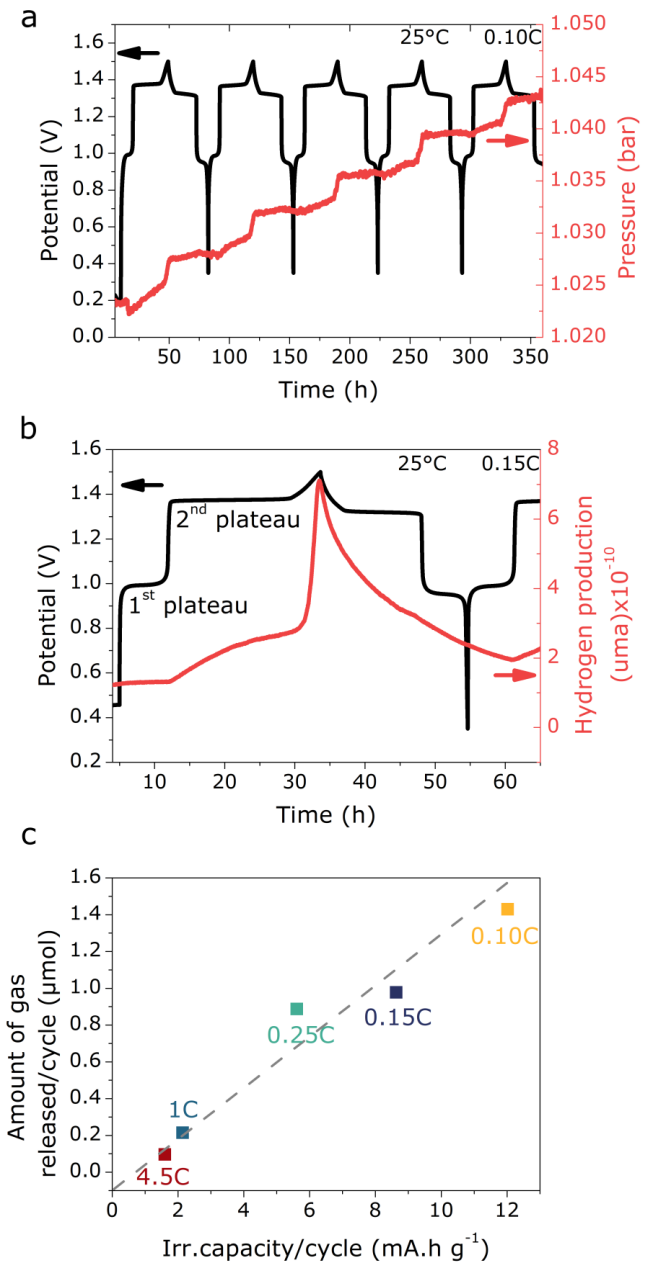


Figure 3. Gas monitoring of Mo_6S_8/$LiFePO_4$ full cell in 20 m LiTFSI. (a) Potential and pressure as a function of time at 0.10C monitored in a pressure cell. (b) Potential and hydrogen evolution as function of time at 0.15C monitored using OEMS cell. (c) Amount of gas released per cycle as function of irreversible capacity (dash line is a guide to the eyes).

To evaluate further the importance of H_2 gas release, we plotted its amount as a function of irreversible capacity per cycle for several C-rates (**Figure 3c**) and note a nearly linear trend with, at 0.1C, an irreversible capacity of 12 mAh g^{-1} that corresponds mainly to a gas release of 1.4 µmol in addition to the contribution of other side reactions. Such an H_2 evolution originates from the

decomposition of H_2O that could proceed either via a direct or indirect process according to reactions 1 and 2 (see detailed equation in Supplementary information), respectively.

$$Direct\ HER:\ 2 \cdot H_2O + 2 \cdot e^- \rightarrow 2 \cdot HO^- + H_2 \quad (1)$$

$$Indirect\ HER: Li_xMo_6S_8 + x \cdot H_2O \rightarrow Mo_6S_8 + x \cdot Li^+ + x \cdot HO^- + \frac{x}{2} \cdot H_2 \quad (2)$$

On the basis of the direct mechanism (reaction 1), we can from a simple calculation nearly account for the amount of H_2 released (see **Figure S 2**, **Table S 2** and **Table S 3** in Supporting Information for detailed calculations), hence implying that reaction 1 is by far majority in the total irreversible capacity (70% of the irreversible capacity per cycle). However, to interrogate the contribution of the indirect mechanism (reaction 2), we measured the self-discharge of a fully charged half-cell by monitoring the variation of the potential over time (**Figure 4**). Nearly 700 hours are needed to reach the end of the de-insertion plateau at 1.3 V *vs.* Li^+/Li, which accounts for a loss of 75 % of the total capacity. Moreover, the self-discharge time is dependent on the C-rate applied in charge and thus on the time spent to form the SEI (Figure 4b), which will inherently define the thickness and density of the SEI thus formed. Such observation demonstrates that the indirect mechanism for water consumption, which is partially reversible in terms of lithium balance, is very slow when compared to the direct one. To quantify the importance of each reaction to the overall water consumption, we calculated the rate of water consumption associated with each reaction taking into account the time, the mass of active material and the H_2 release (see **Table S 4**, **Table S 5** and **Table S 6** in Supporting information).We found that the indirect mechanism (reaction 2) is responsible for the consumption of *ar.* 0.1 % h^{-1} g^{-1} of the total water amount. This rate contrasts with the 0.25 to 0.45 % h^{-1} g^{-1} rate estimated for the direct mechanism (reaction 1). Bearing in mind that a 21 m LiTFSI electrolyte operates at the limit of solubility of the salt (ar. 5 M), such water consumption rate can lead to severe drying out of the cell upon cycling and/or storage.

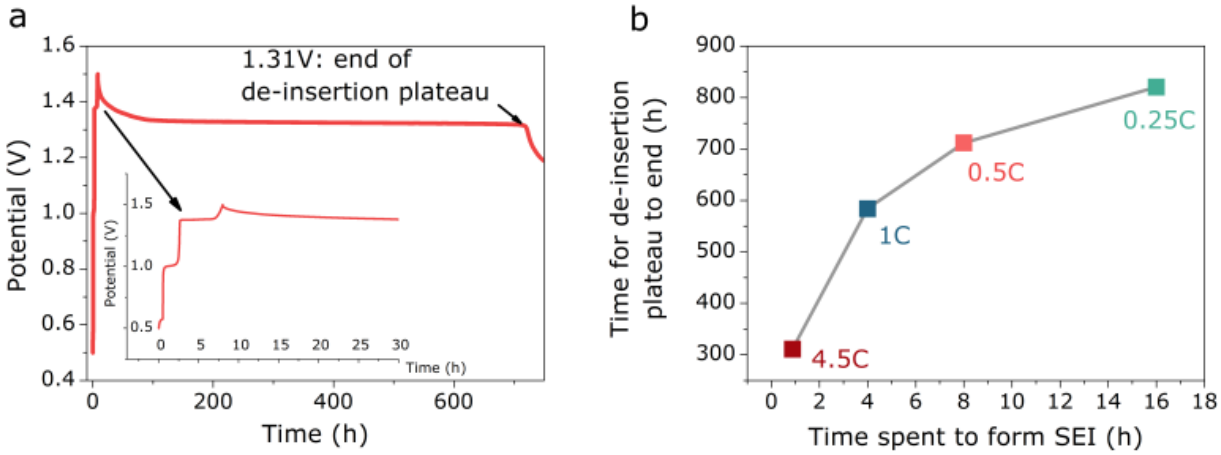


Figure 4. Electrochemical storage of Mo_6S_8/$LiFePO_4$ in 20 m LiTFSI. (a) OCV decay measured for a fully charged cell during rest at 0.5C. (b) Time needed to end the 2nd insertion plateau during the resting period as function of the time spent to form SEI during charge.

2.2.4 SEI stability

The copious amount of irreversible capacity (70 %) determined upon cycling and associated to HER implies that the SEI forming in the presence of WiSE is not passivating enough and stable. To check this point, the SEI formation was mimicked by cycling a glassy carbon working electrode in a 3-electrodes cell before applying a resting period of 1 hour and perform another cyclic voltammetry (CV) measurement to measure the cathodic current corresponding to the HER (**Figure 5a**). During the first CV scan, a peak at 0.75 V *vs* Li^+/Li is observed, and is attributed to HER on the surface of the glassy carbon working electrode.[30][40] Upon cycling, the intensity of this peak decreases before to eventually almost vanish after 15 cycles (see green line). This phenomenon is explained by the gradual passivation of the glassy carbon electrode as a result of the SEI formation, as proposed by Dubouis *et al.*[30] and schematized in **Figure 5b**. However, after applying a 1 hour resting period, the subsequent CV recorded (purple dash line) attests that the passivation is lifted as the peak intensity corresponding to the HER is back to that recorded during the very first cycle. This experiment was also performed at 35 °C, 45 °C and 55 °C and similar trends were observed: the SEI dissolved during resting period, further confirming our self-discharge measurements (Figure 4). Moreover, a competition between the precipitation of LiTFSI, as recently proposed,[40]

and the dissolution of LiF can contribute to this dynamic SEI behavior. However, bearing in mind that the ratio volume of the electrolyte/active material is greater in this experience that in a practical battery, more than 1 hour OCV would be needed to partially dissolve the SEI and suppress its passivation in a full cell. Hence, in practice, self-discharge takes several hundreds of hours, as seen Figure 4a. In conclusion, operando gas monitoring and SEI stability assessment highlight critical limitations associated with the use of superconcentrated electrolytes in terms of Coulombic efficiency and shelf-life. Furthermore, these kinetic-driven limitations are expected to even be greater at elevated temperatures as we tested next.

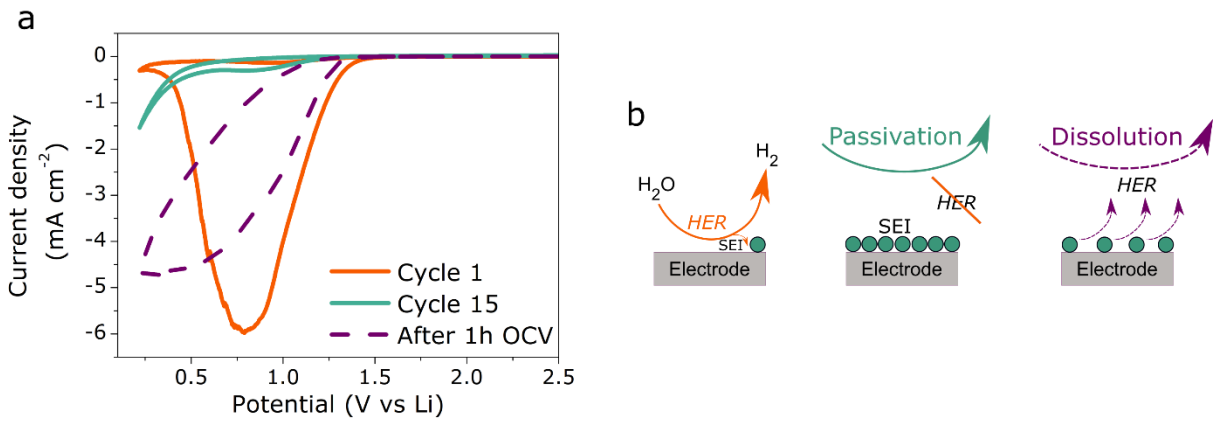


Figure 5. Assessment of the SEI stability over time by mimicking its formation on inert material in 20 m LiTFSI electrolyte. (a) Cyclic voltammetry performed at 50 mV s^{-1} in a 3-electrodes cell using glassy carbon as working electrode, Pt wire as counter electrode and silver wire as pseudo-reference. The first (red) and the fifteenth (green) voltammograms are shown, as well as the one recorded and after 1 hour OCV. (b) Illustration of the SEI formation and its partial dissolution after a resting period of 1 h.

2.2.5 Practical consequences of temperature on cell performances

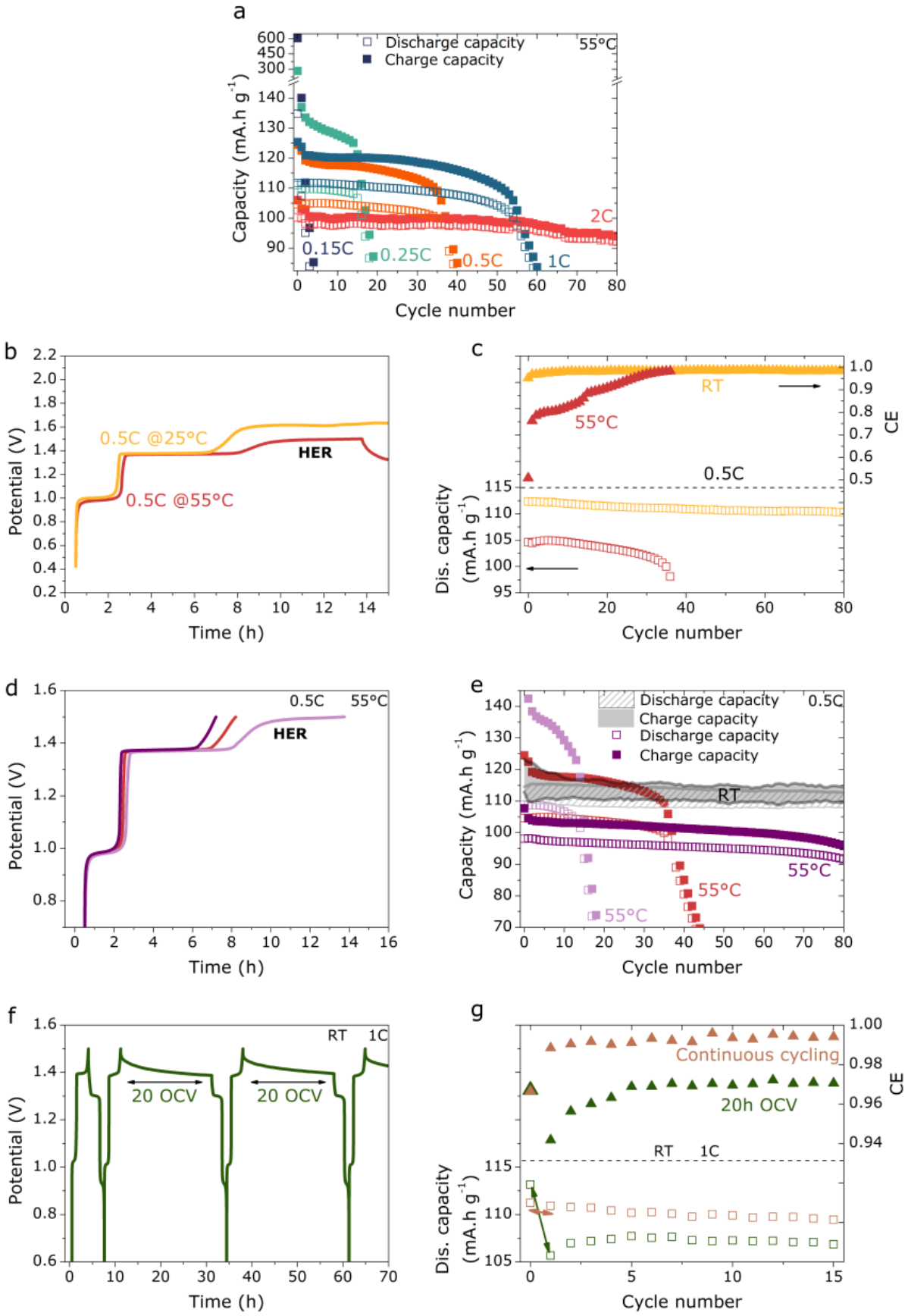


Figure *6*a reveals that the effect of the temperature is more pronounced at low C-rate than at C-rate above 1C. Indeed, an operating temperature of 55 °C leads to a rapid decay of the reversible capacity and a drastic drop of the Coulombic efficiency, both leading to a shorter lifetime for the

battery at low C-rate. Moreover, we can observe at 55 °C a better charge capacity at the beginning of cycling associated with lower Coulombic efficiency (see

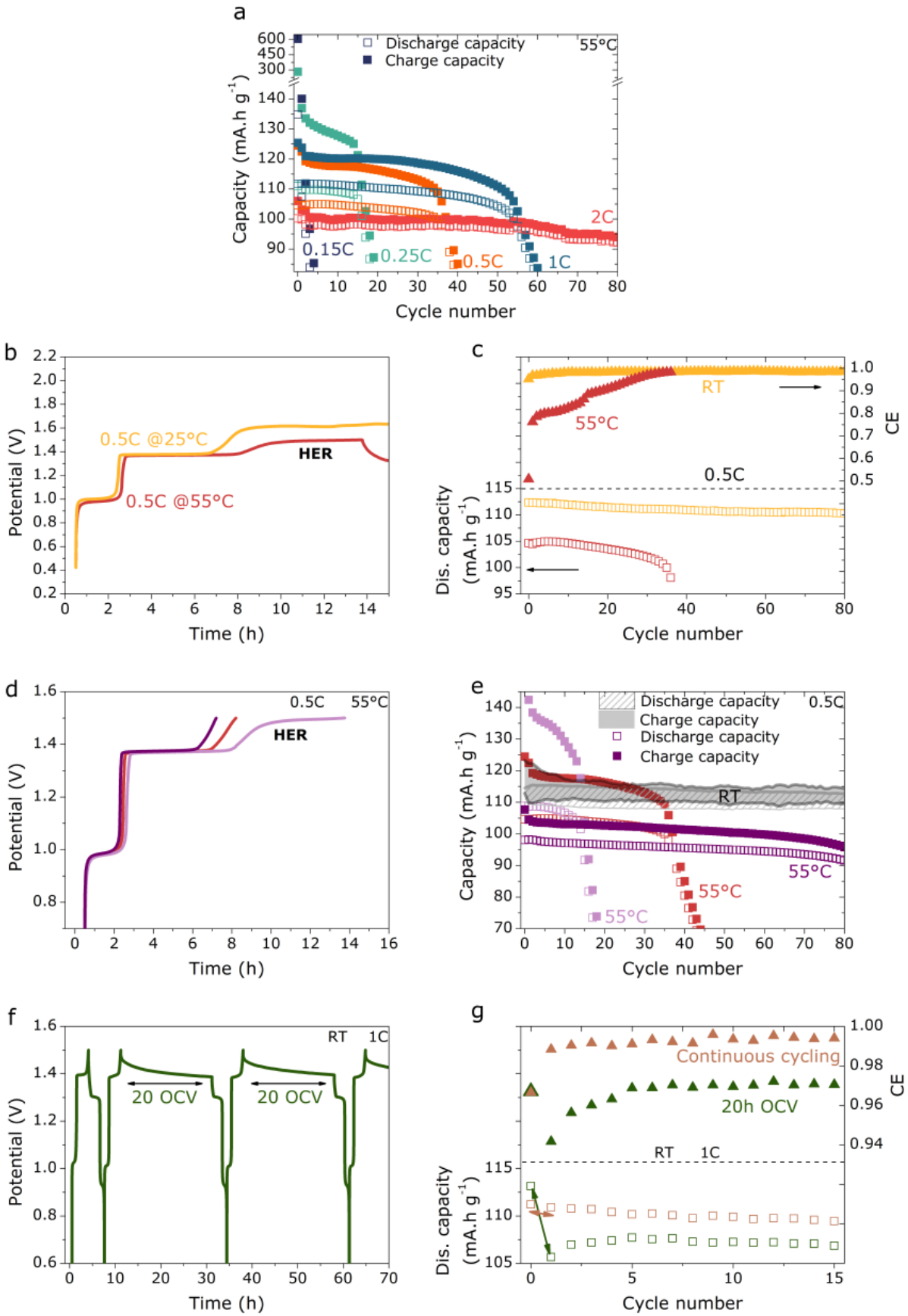


Figure *6*a and **Figure 6b**), demonstrating a greater amount of parasitic reactions at higher

temperatures as evidenced by OEMS measurements (see **Figure S 3**). Besides the enhancement of the global degradation of the cell (loss of electrical contact, faster aging of materials, etc.) at high temperatures, the origin for this phenomenon can be either kinetics or thermodynamics. On the kinetics side, a higher temperature will enhance both the HER kinetics, as well as the SEI dissolution rate for SEI-components such as LiF, LiOH or Li_2O as reported in literature.[20][30] On the thermodynamics side, note that the HER potential shifts towards lower potential by 160 mV between 25 °C and 55 °C ($E_{HER\ @25\ °C}$ = 2.16 V *vs.* Li^+/Li and $E_{HER\ @55\ °C}$ = 2 V *vs.* Li^+/Li), while the Li insertion potential for Mo_6S_8 only shifts by 20 mV (see

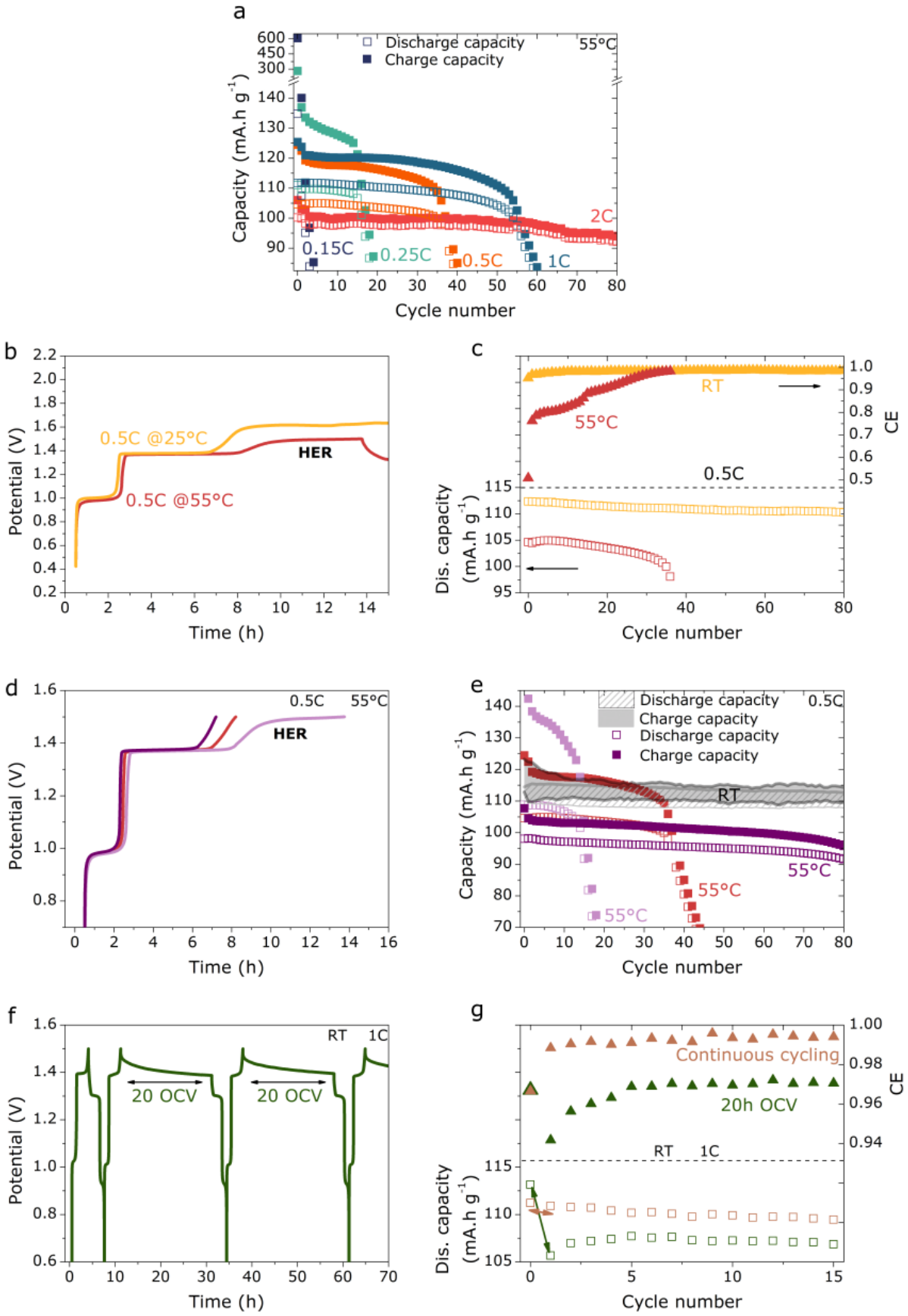


Figure *6c*). This difference leads to the appearance of a plateau attributed to the HER before the cell potential reaches the cut-off, as we could observe for some cells cycled at 0.5C (see

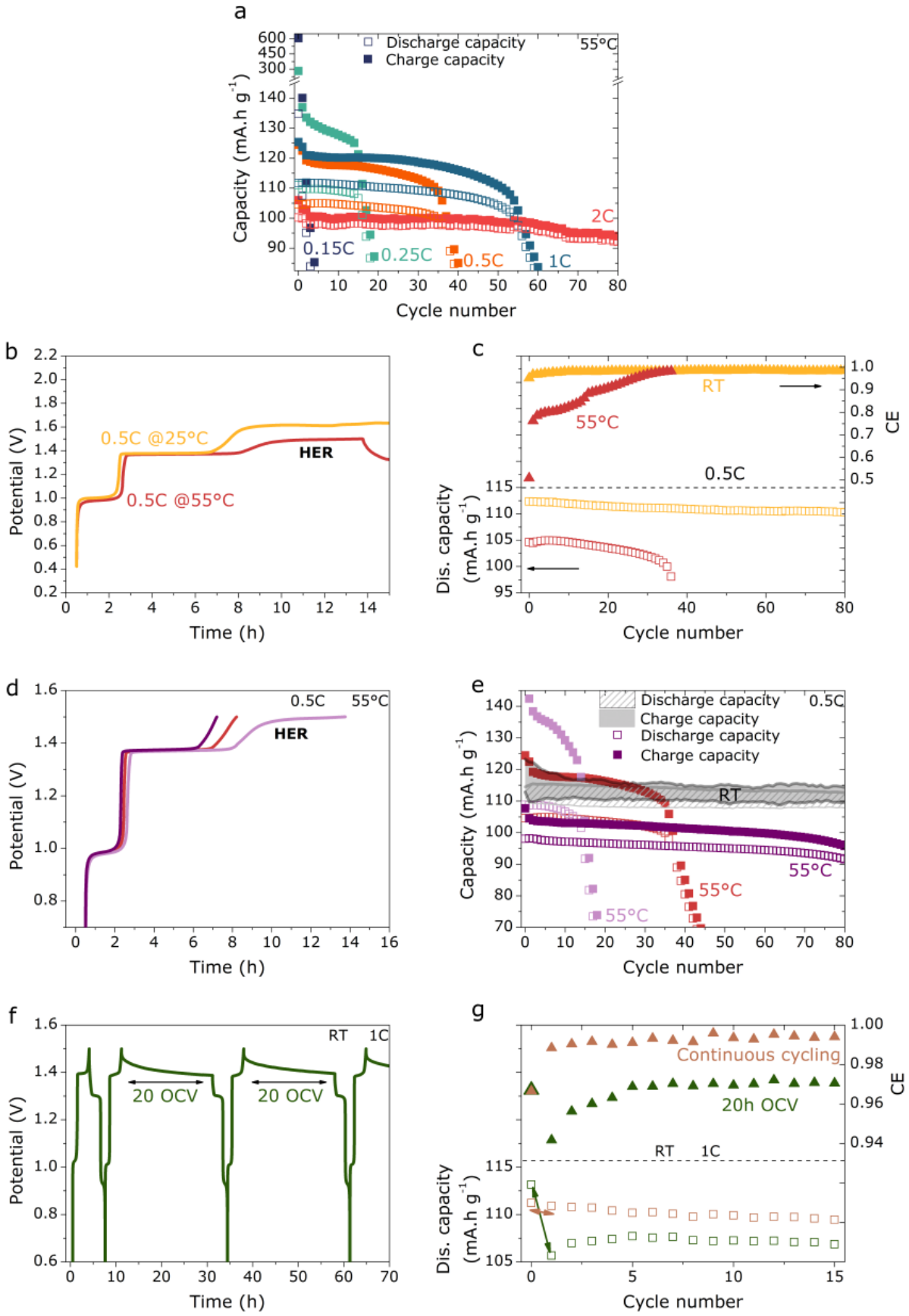


Figure *6*d). Last, it is worth noting that unlike at 25 °C, our results at 55 °C (capacity *vs*. cycle number) for 3 different cells are quite spread (**Figure 6e**). This phenomenon is rooted in the effect of temperature that exacerbates small variations in the SEI formation and stability, which in turn

leads to different microstructures (thickness and density) and thus solubility rate when cycled at 55 °C.

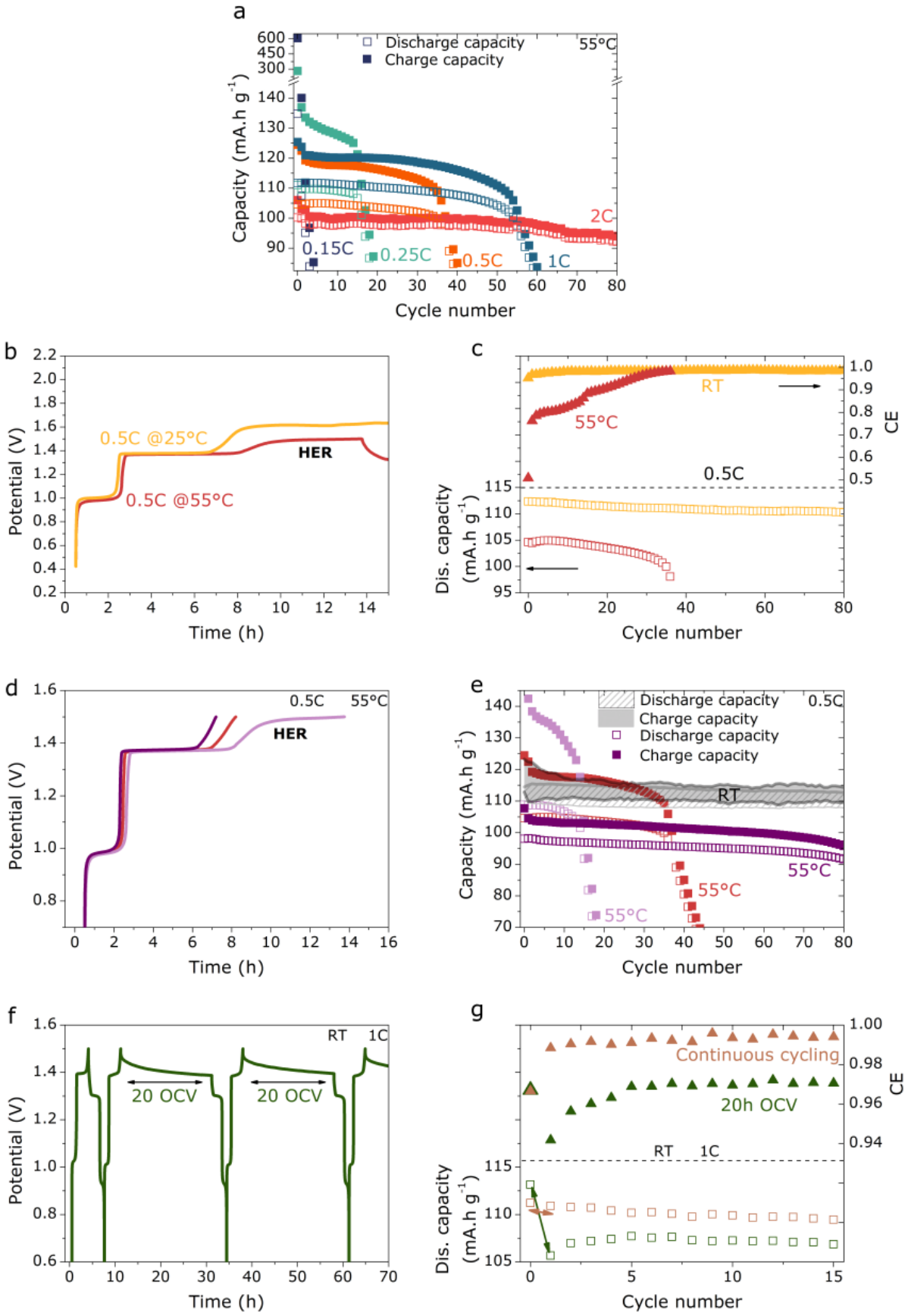


Figure 6. Practical consequences of temperature and self-discharge tests on the life of a Mo_6S_8/LFP cell in 20 m LiTFSI. (a) Charge and discharge capacities as a function of cycle number at 55 °C for several C-rates. (b) Comparison between charge and discharge capacities and Coulombic efficiency as a function of cycle number for cells cycled at 0.5C at 25 °C (yellow) and 55 °C (pink). (c) Potential as a function of time for cells cycled at 0.5C at 25 °C and 0.5C at 55 °C showing the shift of the HER

plateau shift depending on the temperature. (d) Potential as a function of time for 3 cells cycled in same conditions, at 0.5C and 55 °C, showing the poor reproducibility of cell performances at elevated temperature. (e) Charge and discharge capacities as a function of cycle number for 3 cells cycled at 0.5C at 55 °C and range of values for 3 cells cycled at 0.5C and 25 °C that fall with the shade grey area. (f) Potential as a function of time at 1C during the charge/storage protocol. (g) Coulombic efficiency and discharge capacity as function of cycle number for a cell undergoing charge/storage protocol (green) and continuous cycling (brown) at 1C.

2.2.6 Assessing battery self-discharge

Self-discharge was estimated using coin cells according to the following cycling protocol. Briefly, the cells were first charged, discharged and charged at 1C and rested for 20 hours at OCV, this OCV step being repeated at the end of each subsequent charge (see **Figure 6f** for an illustration of the testing protocol). The discharge capacity obtained following this procedure is reported in

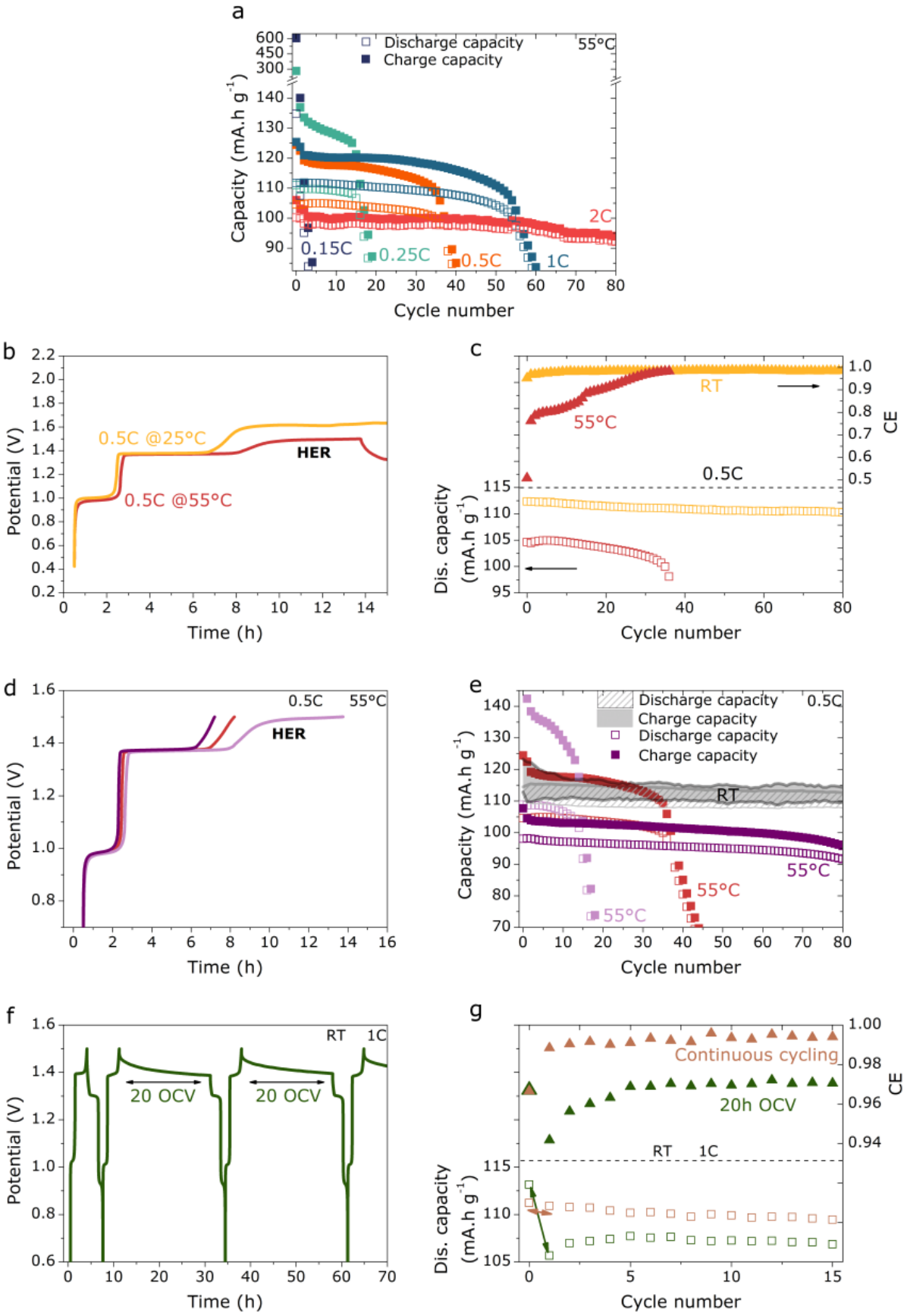


Figure *6g* and compared with that measured with no resting step. Doing so, after the first resting period, a drastic drop of capacity of about 9 mAh g^{-1} is observed, which can be linked to a partial dissolution of the SEI enabling self-discharge. Moreover, in the subsequent charge/storage cycles,

both the Coulombic efficiency and the discharge capacity stabilizes around 97 % and 107 mA.h g^{-1}, respectively - values close from the ones obtained after the first 20 h at OCV (94 % and 105 mA.h g^{-1}) (see Figure 6g). Hence, while the parasitic reactions occurring during the first charge for both protocols are similar (similar Coulombic efficiencies of around 96% during the first cycle), when performing the 20h OCV protocol, the cell degradation is enhanced as a result of the extended period spent at OCV. A similar experiment carried out at 55 °C shows an identical trend with an even more significant loss in capacity (see **Table S 7** in Supporting Information). This result is consistent with a faster SEI dissolution and enhanced HER kinetics at 55 °C, both leading to an increased drop in cell performances. However, these observations contrast with a report published in 2016 by Suo *et al.*. [41] In this publication, self-discharge is assessed after a resting period of 10h following a SEI formation step consisting of 10 cycles performed at 0.5C. A steady increase of the Coulombic efficiency following the 10 hours spent at OCV is observed, as reproduced in **Table S 8** (Supporting information). It suggests that the SEI stability/instability against dissolution depends upon its formation. To explore further this aspect, we replicated the same protocol at room temperature and 55 °C (see **Figure S 4**) and reach a Coulombic efficiency that stabilizes after 3-4 cycles at 98 % and 87 %, respectively, while 30 cycles are required to reach the same Coulombic efficiency as reported in Suo's report.[41] Bearing in mind that protocols are identical, such differences most likely come in the making of the electrodes or in the morphology of the electrode materials. However, we found a constant loss of capacity of about 5 mAh g^{-1} at room temperature while this capacity loss, initially of 6 mAh g^{-1} after the first resting period, decreases on the subsequent resting periods in Suo's report. Moreover, our results stress a loss of capacity upon resting which is not perfectly reversible since the cell discharge capacity smoothly decay upon cycling. Altogether, these data suggest that the SEI cannot fully prevent the HER, therefore explaining that we cannot outpass the 98 % of Coulombic efficiency. Therefore, while optimizing the formatting conditions can help delaying the solubility of the SEI as intensively

experimented in non-aqueous Li-ion batteries, this certainly will not prevent the drying out of the cell over prolonged time, especially at temperature greater than room temperature.

2.3 Use of *Water-in-bisalt* electrolyte: effect on the negative electrode

Altogether our results show that WiSE-based electrolyte cannot lead to a fully protective SEI against the HER occurring during cycling or resting period, hence leading to limited cycling performances. To check if this issue is common to superconcentrated electrolytes, we then explored a bisalt-based electrolyte previously reported by Yamada *et al.,* [4] that shows a wider electrochemical stability window, thus enabling the use of low potential anodes with greater specific and energy density.[4][26]–[28] Consequently, we have benchmarked a 20 m LiTFSI: 8 m LiBETI electrolyte against SEI stability/HER using similar testing protocols as previously used for WiSEs.

Combined OEMS and pressure cell measurements were first performed to both qualitatively and quantitatively assess the effect of gas evolution on cell performances. The potential and the pressure changes plotted as a function of time during cycling (**Figure 7a**) show that the cell pressure continuously increases during cycling, as the result of the evolution of H_2 spotted by OEMS measurement (**Figure 7b**). Hence, alike for WiSE electrolyte, continuous water consumption occurs in parallel with lithium insertion for bisalt electrolyte 20 m LiTFSI: 8 m LiBETI. Furthermore, the contribution of direct HER (**Figure 7**) to the total irreversible capacity is again estimated of at least 70 % (see details of the calculation in Supporting Information). This ratio suggests that the nature of parasitic reactions taking place in WiBS electrolyte is identical to the one in WiSE. Therefore, such a system will certainly face similar issues to WiSE electrolyte, with nevertheless a decreased amount of hydrogen evolution (see discussion below).

We then turned our attention to the stability of the SEI formed in this electrolyte following the same methodology as previously used for WiSE (**Figure 7c**). Doing so, the dissolution of the passivation layer formed on the surface of the glassy carbon electrode after performing 15 scans

(by cyclic voltammetry) was found to occur after 1 hour of resting period, alike for WiSE (Figure 5). Moreover, the SEI dissolution in WiBS electrolyte was definitively confirmed by carrying out a charge/storage protocol (**Figure 7d**) during which the discharge capacity loss observed after a 20 hours OCV period applied after a first cycle is found identical to the discharge capacity loss measured in WiSE, *i.e.,* around 9 mA.h g^{-1}.

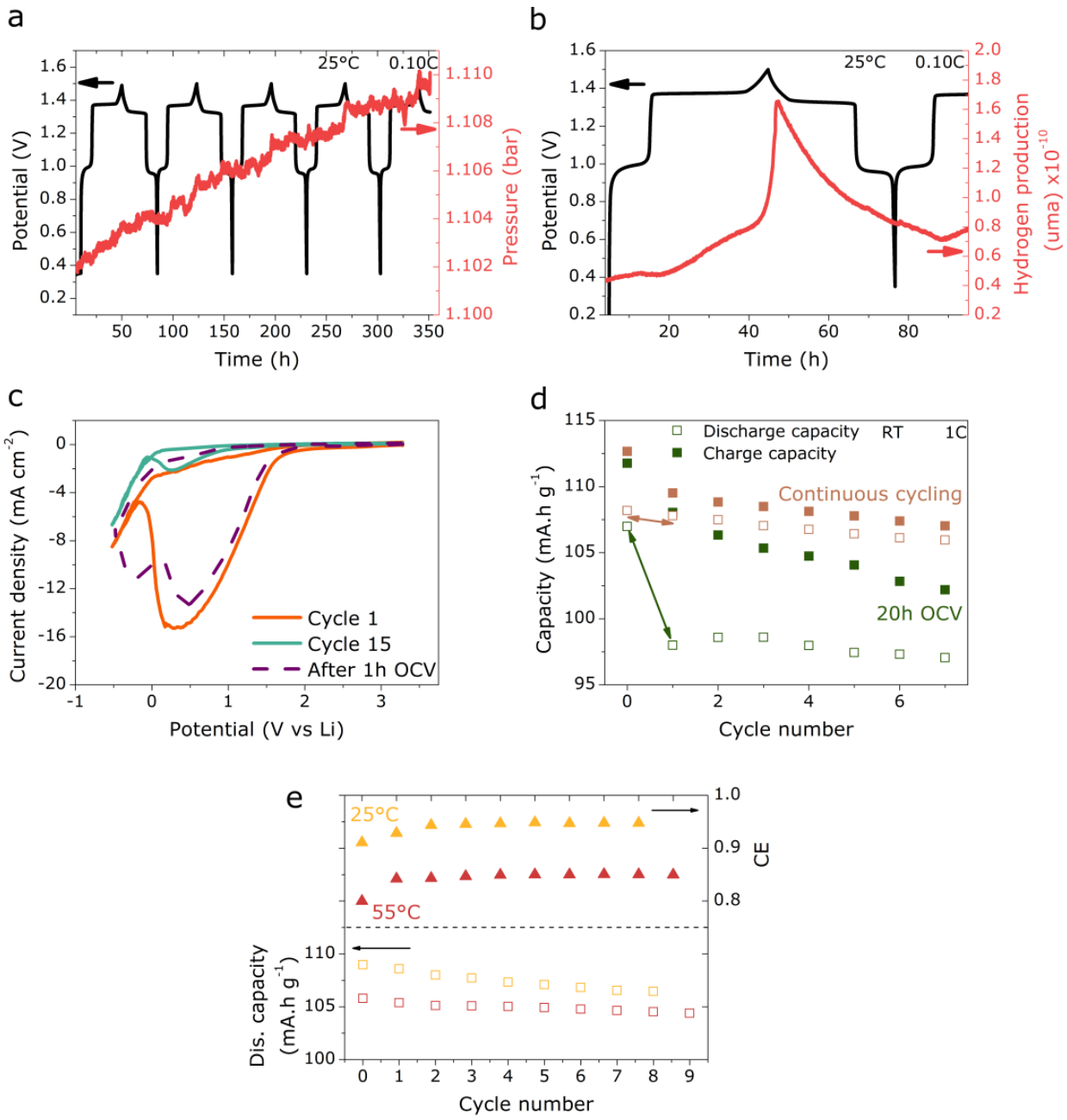


Figure 7: Gas monitoring and practical performances for a Mo_6S_8/LFP battery using 20 m LiTFSI: 8 m LiBETI superconcentrated aqueous electrolyte. (a) Potential and pressure as function of time at 0.10C monitored using a pressure cell. (b) Potential and hydrogen evolution as function of time at 0.10C monitored using an OEMS cell. (c) Cyclic voltammetry performed at 35 °C (to avoid crystallization) at 50 mV s^{-1} in a 3-electrodes cell using glassy carbon as working electrode, Pt wire

as counter electrode and saturated calomel electrode as reference. The first (red) and the fifteenth (green) voltammograms are shown, as well as the one recorded and after 1 hour OCV. (d) Coulombic efficiency and discharge capacity as a function of cycle number for a cell undergoing charge/storage protocol (green) and continuous cycling (brown) at 1C (values are the average calculated with 3 cells). (e) Comparison between charge and discharge capacities and Coulombic efficiency as a function of cycle number for cells cycled at 0.15C at 25 °C (yellow) and 55°C (pink).

Cycling performances were then tested at 55 °C (**Figure 7e**). Doing so, an increase of temperature was found to lead to greater capacity in charge associated with lower Coulombic efficiency, in agreement with an increased amount of parasitic reactions occurring at high temperature due to faster HER kinetics, greater HER onset potential and faster SEI dissolution rate combined with an enhancement of the global degradation of the cell (loss of electrical contact, faster aging of materials, etc.). While all these measurements are very much in line with those previously obtained for WiSE, the capacity fading is nevertheless found to be much slower when using WiBS electrolyte than with WiSE (**Figure S 5**), leading to longer shelf-life. Bearing in mind that the concentration of water in WiBS is 1.6 times smaller than in WiSE, this observation could at first be explained by a decrease of the number of water molecules available for the HER and the dissolution of the SEI in WiBS.[29],[42] However, this explanation is contradicted by recent studies showing that water molecules reduced in the HER process are those solvating lithium cation[44] and that the first solvation sheath of lithium cation is rather similar in WiSE and WiBS, therefore the reactivity of water in these two electrolytes should be alike.

A more likely possibility is the viscosity difference between both electrolytes that is about 6 times greater for WiBS (203 mPa.s at 30°C[4]) than for WiSE electrolyte (36.2 mPa.s at 25°C[3]). The higher viscosity would limit the HER kinetics and the dissolution rate of the SEI, thus enabling better performances. Moreover, independently of the change in viscosity and therefore of the change in solubility of the inorganic species forming the SEI, electrolyte saturation is most probably never reached when forming a few nanometer thin protective layer on the electrode

surface. This is consistent with the observation of a similar capacity fading at room temperature, after 20 hours of rest, for two coin cells using WISE and WiBS electrolytes.

Altogether, these results show that WiBS-based battery faces critical limitations identical to the ones encountered for WiSE with the exception of offering a better capacity retention at 55°C. However, Li-aqueous battery using WiBS, alike for WiSE, are penalized practically-wise by the absence of the formation of a self-passivating SEI upon cycling; a drastic difference with aprotic Li-ion batteries whose excellent performances are ensure by a protective SEI.

2.4 Effects of WiSE and WiBS on the positive electrode gassing

Besides the SEI forming at the negative electrode, another important aspect in selecting electrolytes regard their stability at the positive electrode under highly oxidizing potentials. Having established above that the cycling performances for WiSE-based aqueous batteries will certainly be limited by the absence of stable SEI at the negative electrode, we focused our attention on gassing experiments rather than on cycling performances for the positive electrode.

Figure 8. Potential and pressure measured as a function of time for NMC622/LTP cells cycled in (a) Water-in-salt 20 m LiTFSI electrolyte at 25 °C, (b) at 55 °C (*note that the peak observed below 80 hours for the pressure is due to an opening of the oven) and (c) Water-in-bisalt 20 m LiTFSI:8 m LiBETI at 55 °C.**Figure 8a** shows the evolution of pressure and potential as a function of time for a LTP/NMC_{622} cell using WiSE electrolyte at 25 °C. There, even when pushing the potential cut-off up to 2 V (4.78 V *vs.* Li^+/Li), any pressure increase can hardly be detected, with only a pressure increase of 0.6 mbar (0.22 µmol of gas) being observed, this amount being within the detection limit of this technique. This absence of gassing is consistent with the previously reported formation of a TFSI-rich double layer, preventing water to access to the interface. Furthermore, this observation is also consistent with the OER kinetics being very sluggish when compared to the HER, as widely discussed in the electrocatalysis field.[42] Hence, at 25 °C, WiSE electrolyte seems to

be stable and not to face any drastic degradation, in agreement with the electrochemical stability of superconcentrated aqueous electrolytes under anodic polarization reported in previous studies.[4][43]

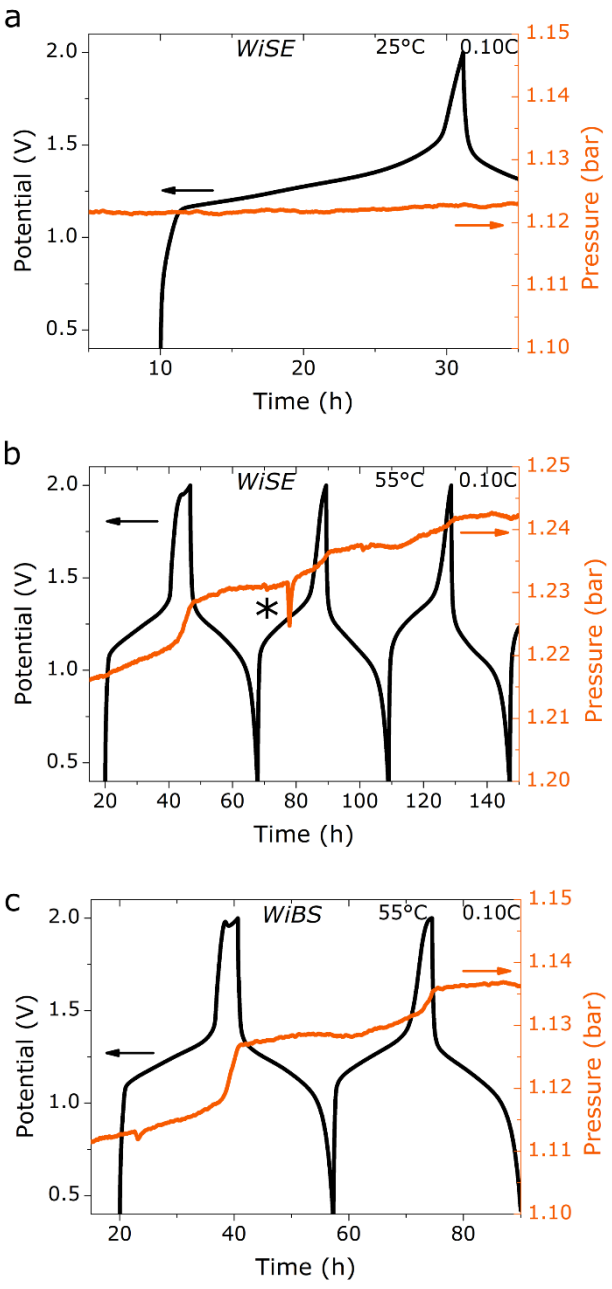


Figure 8. Potential and pressure measured as a function of time for NMC_{622}/LTP cells cycled in (a) *Water-in-salt* 20 m LiTFSI electrolyte at 25 °C, (b) at 55 °C (*note that the peak observed below 80 hours for the pressure is due to an opening of the oven) and (c) *Water-in-bisalt* 20 m LiTFSI:8 m LiBETI at 55 °C.

Following these measurements at room temperature, the anodic stability of WiSE was assessed at higher temperature by cycling pressure cells at 55 °C. The evolution of pressure and potential as a function of time are reported in **Figure 8b**. Compared to the results obtained at room temperature, a significant gas evolution could be spotted during delithiation/oxidation of NMC_{622} with two slopes being observed. The first one that leads to a pressure increase of 4.3 mbar (1.59 µmol) occurs between 1.1 V and 1.4 V, and can be explained by the competition between the electrochemical Li^+ de-intercalation and the slow parasitic reactions, either direct (OER) or indirect (self-discharge).[44] The second one starting above 1.4 V (4,2 V *vs.* Li^+/Li) leads to a greater production of gases of ar. 7 mbar (2.59 µmol) and can be mainly attributed to parasitic reactions, which can also be responsible for the appearance of a plateau at high potential (*ar.* 2 V) which is solely present during the first charge. Indeed, NMC is known to face greater degradation at high temperatures and high potential cut-off.[45]–[47] However, the origin of the gas production certainly arises from the corrosion of the carbon additive at high potential in aqueous media, as spotted by OEMS measurements during which CO_2 is detected (**Figure S 6**).[48][49] Nonetheless, the detection of more than one gas, during these measurements, prevents us from performing quantification to determine the amount of mole produced by each gases. For sake of completion, the stability of WiBS-based electrolyte was also tested using pressure cells at 55 °C (**Figure 8c**), and similar behavior is observed as for WiSE. Hence, the pressure increase recorded during the de-insertion plateau between 1.1 V and 1.4 V is around 3 mbar (1.11 µmol) in WiBS, compared to 4 mbar in WiSE. This first gas release is followed by an additional pressure increase of 8mbar (2.96 µmol) at greater potential, compared to 7 mbar previously measured for WiSE. To conclude, at elevated temperature, the stability of the NMC_{622} self-standing electrode/superconcentrated aqueous electrolyte assembly is compromised under anodic polarization when compared to room temperature.

2.5 Discussion and figure of merit for superconcentrated aqueous Li-ion batteries

Based on these experimental results, the figure of merits for WiSEs-based aqueous Li-ion system is compared to those for classical organic Li-ion (NMC_{111} / LP30 / graphite) as well as other aqueous systems (**Figure 9**). As evidenced in our study, WiSEs-based aqueous batteries can only safely operate within a ≈ 2 V operating window to avoid parasitic side reactions, unlike organic Li-ion batteries. To be able to compare our WiSE or WiBS-based battery to classical Li-ion or commercial aqueous systems, we estimated both the energy density and the specific energy for WiSE and WiBS following the protocol proposed by Betz *et al.*[50] In this protocol, values are estimated for Li-ion battery based on lab-scale measurements (in Swagelok or coin cells) by extrapolation of the electrode materials loading and the electrolyte volume usually employed for 18650 cells. The details for these calculations are given in the Supplementary Information. Thus, both the specific energy density and the energy density at a cell level are twice smaller than for aprotic Li-ion batteries and eventually similar to the ones achieved by nickel-metal hydride (Ni-MH) batteries, while being above those for Ni-Cd or Lead-acid batteries. However, the energy efficiency is similar/close to the one obtained for Li-ion (> 90 %), unlike Lead-acid, Ni-Cd, and Ni-MH batteries that show energy efficiency closer to 80-85 %.

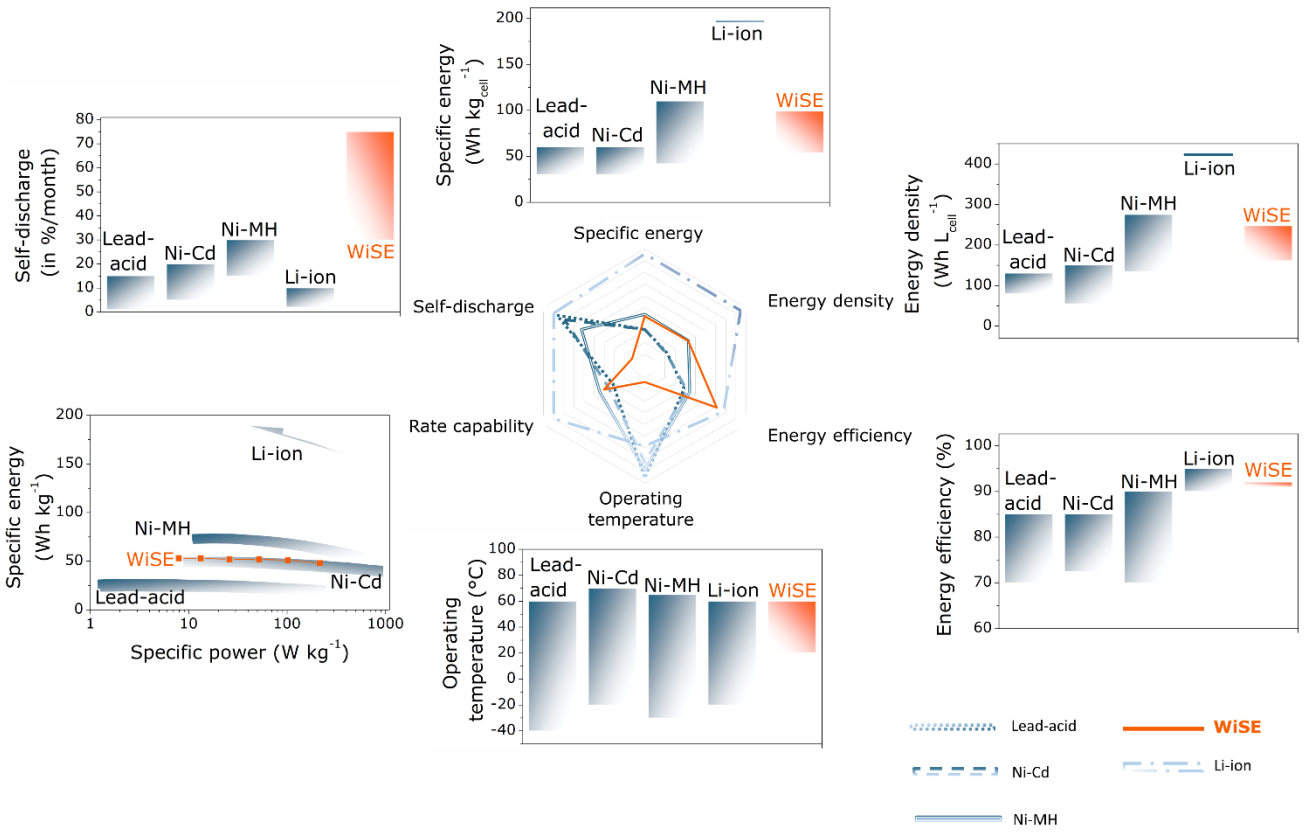


Figure 9. Benchmarking WiSE-based and WiBS-based aqueous batteries against other aqueous systems, namely Pb-acid, Ni-Cd and Ni metal hydrides (Ni-MH) batteries as well as against aprotic Li-ion batteries. The spider-chart at the center compares these systems in terms of six parameters defining the overall performances of these systems. On top is compared the specific energy for these systems, on the left the self-discharge for these systems, on the right the energy density, on the bottom left is represented the specific energy as a function of specific power, on the bottom right is reported the energy efficiency for these systems while on the bottom the operating temperature window for the different technologies. All references are given in Supporting information.

Evidently, cycling aqueous batteries within the thermodynamically stable potential window of water drastically limits the energy density, which cannot reach the one achieved by Li-ion batteries. The obvious way to increase the energy density would be to extend the operating window beyond the stability window, alike other aqueous batteries (Pb-Acid), while finding chemical-engineering means to handle the gas generated during cycling. For vented Lead-acid batteries, a catalyst such as Pd can be added in the form of a battery plug to catalyze the $H_2 + ½ O_2 = H_2O$ gas recombination reaction and minimize the electrolyte loss and thus the dry-out of the cell. Similarly, catalysts are added for vented Ni-Cd batteries to help recombine gases and

minimize the loss of water from the electrolyte. Hence vented WiSE aqueous batteries could be envisioned, providing that the salt crystallization issue discussed by Kühnel *et al.*[35] can be solved for superconcentrated electrolytes, as upon continuous consumption of water, the battery lifetime will rapidly reduce.

An alternative approach to circumvent the electrolyte drying-out can be the design of sealed WiSE-based batteries. For Lead-acid batteries, the so-called Valve Regulated Lead Acid (VRLA) sealed batteries were developed using a porous gel-type electrolyte to promote the diffusion of oxygen produced at the positive electrode towards the negative electrode (gases diffuse faster in gel-type electrolyte than in liquid aqueous electrolytes), where it recombines to form H_2O, thus forming a so-called "oxygen cycle".[51] For sealed Ni-Cd and Ni-MH battery, recombination of oxygen into water is also performed. However, the right balance between the capacity of the negative electrode vs. that of the positive must be ensured to enable the recombination of oxygen without promoting the HER, *e.g.*, ensuring that the positive electrode reaches full capacity before the negative faces HER. If no care about the dimensionality of the electrodes is taken, as for commercial Lead-acid, Ni-Cd and Ni-MH, aqueous-based batteries face an unbalanced generation of gases and poor recombination efficiency. Furthermore, for safety reasons, catalysts such as Pt/Pd are also employed to help hydrogen recombination (when needed) by reacting with oxygen produced during self-discharge.

However, the development of these different concepts would (i) need electrolyte refill to avoid drying-out of the cell or (ii) require the use of catalysts to recombine water from $O_{2(g)}$ and $H_{2(g)}$ and/or (iii) of a gelified electrolyte to improve gas diffusion. Therefore, these constraints would impose drastic limitations regarding both the operating voltage as well as the charging rate for WiSE-based aqueous batteries. Indeed, both increasing the operating voltage and increasing the charging rate would lead to increased kinetics for gas generation. For instance, as observed for Ni-Cd batteries, water recombination catalysts can only handle a certain amount of gas, which limits

the charging to 0.1C. Moreover, the water recombination in these aqueous devices requires a sufficient amount of oxygen to allow recombination. Indeed, these systems rely on the paradox that a too good positive electrode for which no oxygen is released would not allow for the water recombination at the negative electrode. However, as evidenced in our study, while hydrogen is produced in parallel with lithium intercalation at the negative electrode during charge, almost no oxygen is released at the positive electrode at room temperature. This unbalanced generation of gases between the positive and the negative electrode towards the generation of hydrogen, which is not encountered for other aqueous devices, drastically limits the possibility of water recombination in WiSE-based aqueous batteries, eventually leading to severe drying-out issues for the battery.

Furthermore, another major drawback of WiSE-based batteries is the narrow operating temperature range. Indeed, crystallization of the electrolyte may occur at room temperature. Even though several anions have been considered to downshift the crystallization point,[21][24][25][27] the question of the cost, scalability and the competitiveness of the superconcentrated aqueous electrolyte will be raised. With this in mind, reducing further the amount of water by increasing the amount of lithium salt in the electrolyte does not appear as a viable solution for applications competing with Li-ion batteries. Indeed, as we demonstrated in our work, the SEI dissolution is not suppressed by the use of bisalt superconcentrated electrolytes.

Finally, for grid applications, the capacity fading of WiSE-based batteries must be limited over time. However, as shown in our work, the second intercalation plateau of Mo_6S_8 corresponding to 75 % of the total capacity of the material is completely loss after a resting period of 300 to 800 hours, depending on the C-rate employed during cycling. Thus, capacity fading in the order of 30 to 75% per month is deduced for this specific configuration, which must be compared with capacity fading of 2-10 % measured for aprotic Li-ion batteries, 1-15 % for Lead-acid batteries, 15-30 % for Ni-MH and 10-20 % for Ni-Cd, bearing in mind than some can be recovered for

commercial Ni-Cd and Ni-MH aqueous systems as well as for WiSE-based system. Thus, without further improvement to the current technology and the finding of optimized precycling conditions, WiSE-based aqueous batteries cannot currently be regarded as a viable option for grid electricity storage.

3. Conclusion

We have reported an in-depth study of the cathodic and anodic stability of superconcentrated aqueous electrolytes as a function of the operating conditions. Doing so, we concluded that the SEI formed in these superconcentrated electrolytes is not protective enough to prevent the electrolyte degradation during cycling and resting period, more specifically to avoid water reduction and hydrogen generation. Furthermore, self-discharge as well as capacity fading were observed during storage. Finally, we found that at elevated temperature, these parasitic reactions are exacerbate.

Based on these experimental results, we provide the figure or merit for WiSE-based Li-ion battery that we compared to that of classical Li-ion battery and commercial aqueous system such as Lead-acid, Ni-Cd or Ni-MH. Doing so, it clearly appears that while WiSE-based batteries share the energy efficiency of aprotic Li-ion batteries, owing to similar intercalation reactions, it only offers the energy density and the specific energy of Ni-MH batteries. However, WiSE-based batteries show poorer temperature stability than either systems. Furthermore, the continuous electrolyte consumption occurring both on charge and upon self-discharge for WiSE-based batteries may lead to the drying-out of the cell. Our analysis further revealed that owing to the lack of oxygen generation upon charge, the implementation of a gas recombination cycle in WiSE-based cells as used for other aqueous battery applications might be complex. Therefore, superconcentrated aqueous electrolyte are currently not able to compete with commercialized aqueous systems for

grid storage application until means to prevent the HER at the negative electrode can be found and benchmarked in practical conditions. This calls for the design of stable and not progressively soluble SEI as reported herein. Over the years, this challenge has been solved with aprotic Li-ion batteries owing to the use of multifunction additives and of coatings and grafting approaches. Could such approaches be as prolific for superconcentrated electrolyte remains an open question. As dealing with aqueous electrolytes does not offer the richness of additives that aprotic systems offer, pursuing the organic coating approach appears more attractive. Whatever, we believe that our study highlights that proper and careful experimental protocols must be adopted in order to assess the practicability of any new battery chemistry. Presently the practical outcome of WiSE within the battery field remains highly questionable. It nevertheless remains that superconcentrated electrolytes may find applications in battery recycling rather than battery assembling as it will be reported elsewhere.

4. Experimental Methods

Electrolyte preparation

Lithium bis(trifluoromethanesulfonyl)imide (LiTFSI, $LiN(SO_2CF_3)_2$) was obtained from Solvay and used as received. Lithium Bis(pentafluoroethanesulfonyl)imide (LiBETI, $LiN(SO_2CF_2CF_3)_2$) was purchased from TCI Chemicals and used as received. 20 mol kg^{-1}, 10 mol kg^{-1} and 5 mol kg^{-1} of LiTFSI electrolyte solutions were prepared by mixing LiTFSI salt and Milli-Q ultrapure water.

Material synthesis and characterization

$LiFePO_4$ (LFP) and $LiNi_{0.6}Mn_{0.2}Co_{0.2}0_2$ (NMC_{622}) were purchased from Umicore. $LiTi_2(PO_4)_3$ (LTP) was prepared by solid-state reaction of stoichiometric amounts of Li_2CO_3 (>99 %, Sigma Aldrich), TiO_2 (>99 %, Sigma Aldrich) and $NH_4H_2PO_4$ (98 %, Alfa Aesar). The precursors were grinded and heated at 200 °C for 2 h and finally 930 °C for 24 h in air. Mo_6S_8 was either obtained from ISCR (Institut des

Sciences Chimiques de Rennes) or homemade synthetized through the following reaction. Mo_6S_8 was prepared by a solid-state reaction of stoichiometric amounts of Cu, Mo (99.95 %, Alfa Aesar) and S (99.98 %, Sigma Aldrich). The precursors were grinded and heated to 700 °C during 24 h and finally 1175 °C for 50 h. Then the resulting sample was acid-leached overnight in HCl 6 M under oxygen. The powder and the supernatant were separated by centrifugation and the samples were washed with distilled water until pH=7, prior to being dried at 80 °C under vacuum overnight.

X-ray diffraction (XRD) was performed to confirm the phases purity using a BRUKER D8 Advance diffractometer with Cu Kα radiation ($\lambda_{K\alpha1}$ = 1.54056 Å, $\lambda_{K\alpha2}$ = 1.54439 Å).

Electrochemical measurement

Electrode preparation

For testing Mo_6S_8, NMC_{622}, LFP and LTP materials, composite self-standing electrodes were fabricated using Bellcore technique. Active materials (AM), Carbon super P (Csp, Timcal) and PVdF-HFP (Solvay) were grinded and mixed in acetone to form a slurry. Ratio used are 73 wt.% of AM, 8 wt.% of Csp and 19 wt.% of PVdF-HFP for Mo_6S_8 and LFP; 60 wt.% of AM, 20 wt.% of Csp and 20 wt.% of PVdF-HFP for NMC_{622} and LTP. NMC_{622} and LTP were mixed with Csp for 20 min using the Spex miller with a ball to powder weight ratio of 11 for LTP and 8 from NMC_{622} prior to be mixed with PVdF-HFP. DBP (Dibutylphtalate, 99 % Sigma-Aldrich) was added to use as plasticizer. Then, the as prepared slurry was casted by doctor blade technique and left to dry overnight. Electrodes were punched with a 0.5 inch diameter and loading of around 7 mg cm^{-2} (Mo_6S_8, NMC_{622}), 9.6 mg cm^{-2} (LTP) or 21 mg cm^{-2} (LFP) of active material were obtained. Finally, electrodes were washed 3 times in diethyl ether (99 %min Alfa Aesar) and dried at 60 °C under vacuum. NMC_{622} electrochemical signature in LP30 was obtained using directly the powder mixture of NMC_{622} and Csp (see Figure 1b).

For the overcapacitive carbon YP50 counter electrodes, self-standing PTFE electrodes were prepared by mixing YP50 and PTFE (1 µm, Sigma-Aldrich) at a weight ratio of 9:1 in isopropanol. The slurry was laminated several times to obtain films of around 20 mg cm^{-2}. Electrodes were dried at 60°C under vacuum.

Cycling tests: galvanostatic experiments

All battery cells were assembled in an Ar-filled glovebox (MBRAUN). Electrolytes were saturated with argon prior to any experiment. Two Whatman glass fibers used as separators were soaked with the electrolyte. Mo_6S_8/LFP (1:4) full cells where assembled using stainless steel as current collectors. LTP/NMC_{622} (1.1:1) full cells were assembled using stainless steel current collector for the negative electrode (LTP) and titanium for the positive one (NMC_{622}).

Concentration, long-cycling and charge/storage tests were performed using coin-cells. Pressure cells tests were performed using a Swagelok-derived cell that integrates a pressure sensor [52]. OEMS measurement was carried out with one homemade cell connected to the mass spectrometer coming from Hiden analytical (HAL 101-RC) [53].

Room temperature electrochemical tests were performed using a BCS-805 potentiostat (Bio-Logic). 55 °C galvanostatic cycling, pressure cells (25 °C) and OEMS (25 °C, 55 °C) experiments were performed in a temperature-controlled oven using a MPG2 multichannel potentiostat (Bio-Logic).

C-rate was set as 1C is equal to one Li cation inserted.

Cyclic voltammetry

Electrochemical stability window (ESW) and SEI stability experiments were performed in an electrochemical glass cell. ESW determination was performed using mirror polished current collector materials (stainless steel or titanium) as working electrode. Pt wire was use as counter electrode and Ag/AgCl reference was used as reference electrode. SEI stability was performed using a PTFE embedded glassy carbon disc (3 mm diameter, Pine Research Instrumentation) as

working electrode and Pt wire as counter electrode. Silver wire was used as *pseudo*-reference. Temperature was controlled by flowing water whose temperature is controlled thanks to a chiller into a mantle around the electrochemical glass-cell.

Li^+ insertion/de-insertion reversibility in active material was tested using a three-electrode PFA Swagelok cell with two glassy carbon rods as current collectors. Self-standing electrodes were used as working electrode, YP50 as counter electrode and Ag/AgCl reference as reference electrode.

Cyclic voltammetry experiments were performed on a VMP3 potentiostat (Bio-Logic). 100 mV s^{-1} scan rate was applied for ESW determination, 50 mV s^{-1} for SEI stability and 1 mV s^{-1} for Li^+ insertion/de-insertion reversibility. All potential were converted *vs*. Li^+/Li scale.

Supporting Information
Supporting Information is available from the Wiley Online Library or from the author.

Conflict of Interest
The authors declare no competing interests

Acknoledgment
L.D. would like to acknowledge the Direction Générale de l'Armement (DGA) for financial support. The authors would like to thank the French National Research Agency for its support through the Labex STORE-EX project (ANR-10-LABX-76-01) and through the project BALWISE (project ID: ANR-19-CE05-0014)

References

[1] W. Li, J.R. Dahn, D.S. Wainwright, *Science* **1994**, *264*, 1115.
[2] Y. Yamada, A. Yamada, *J. Electrochem. Soc.* **2015**, *162*, A2406.
[3] L. Suo, O. Borodin, T. Gao, M. Olguin, J. Ho, X. Fan, C. Luo, C. Wang, K. Xu, *Science* **2015**, *350*, 938.
[4] Y. Yamada, K. Usui, K. Sodeyama, S. Ko, Y. Tateyama, A. Yamada, *Nat. Energy* **2016**, *1*.
[5] J. Han, H. Zhang, A. Varzi, S. Passerini, *ChemSusChem* **2018**, *11*, 3704.
[6] L. Jiang, L. Liu, J. Yue, Q. Zhang, A. Zhou, O. Borodin, L. Suo, H. Li, L. Chen, K. Xu, Y. Hu, *Adv. Mater.* **2020**, *32*, 1904427.
[7] D. Reber, R.-S. Kühnel, C. Battaglia, *ACS Mater. Lett.* **2019**, *1*, 44.
[8] L. Suo, O. Borodin, Y. Wang, X. Rong, W. Sun, X. Fan, S. Xu, M.A. Schroeder, A.V. Cresce, F. Wang, C. Yang, Y.-S. Hu, K. Xu, C. Wang, *Adv. Energy Mater.* **2017**, *7*, 1701189.
[9] Q. Zheng, S. Miura, K. Miyazaki, S. Ko, E. Watanabe, M. Okoshi, C.-P. Chou, Y. Nishimura, H. Nakai, T. Kamiya, T. Honda, J. Akikusa, Y. Yamada, A. Yamada, *Angew. Chem. Int. Ed.* **2019**, *58*, 14202.

[10] H. Chen, Z. Zhang, Z. Wei, G. Chen, X. Yang, C. Wang, F. Du, *Sustain. Energy Fuels* **2020**, *4*, 128.
[11] L. Jiang, Y. Lu, C. Zhao, L. Liu, J. Zhang, Q. Zhang, X. Shen, J. Zhao, X. Yu, H. Li, X. Huang, L. Chen, Y.-S. Hu, *Nat. Energy* **2019**.
[12] D.P. Leonard, Z. Wei, G. Chen, F. Du, X. Ji, *ACS Energy Lett.* **2018**, *3*, 373.
[13] T. Liu, L. Tang, H. Luo, S. Cheng, M. Liu, *Chem. Commun.* **2019**, *55*, 12817.
[14] Q. Dong, X. Yao, Y. Zhao, M. Qi, X. Zhang, H. Sun, Y. He, D. Wang, *Chem* **2018**, *4*, 1345.
[15] S. Chen, R. Lan, J. Humphreys, S. Tao, *ACS Appl. Energy Mater.* **2020**, *3*, 2526.
[16] X. He, B. Yan, X. Zhang, Z. Liu, D. Bresser, J. Wang, R. Wang, X. Cao, Y. Su, H. Jia, C.P. Grey, H. Frielinghaus, D.G. Truhlar, M. Winter, J. Li, E. Paillard, *Nat. Commun.* **2018**, *9*.
[17] J.M. Park, M. Jana, P. Nakhanivej, B.-K. Kim, H.S. Park, *ACS Energy Lett.* **2020**, 1054.
[18] C. Yang, J. Chen, T. Qing, X. Fan, W. Sun, A. von Cresce, M.S. Ding, O. Borodin, J. Vatamanu, M.A. Schroeder, N. Eidson, C. Wang, K. Xu, *Joule* **2017**, *1*, 122.
[19] L. Dai, O. Arcelus, L. Sun, H. Wang, J. Carrasco, H. Zhang, W. Zhang, J. Tang, *J. Mater. Chem. A* **2019**, *7*, 24800.
[20] L. Suo, D. Oh, Y. Lin, Z. Zhuo, O. Borodin, T. Gao, F. Wang, A. Kushima, Z. Wang, H.-C. Kim, Y. Qi, W. Yang, F. Pan, J. Li, K. Xu, C. Wang, *J. Am. Chem. Soc.* **2017**, *139*, 18670.
[21] M. Becker, R.-S. Kühnel, C. Battaglia, *Chem. Commun.* **2019**, *55*, 12032.
[22] J. Vatamanu, O. Borodin, *J. Phys. Chem. Lett.* **2017**, *8*, 4362.
[23] O. Borodin, L. Suo, M. Gobet, X. Ren, F. Wang, A. Faraone, J. Peng, M. Olguin, M. Schroeder, M.S. Ding, E. Gobrogge, A. von Wald Cresce, S. Munoz, J.A. Dura, S. Greenbaum, C. Wang, K. Xu, *ACS Nano* **2017**, *11*, 10462.
[24] J. Forero-Saboya, E. Hosseini-Bab-Anari, M.E. Abdelhamid, K. Moth-Poulsen, P. Johansson, *J. Phys. Chem. Lett.* **2019**, *10*, 4942.
[25] S. Ko, Y. Yamada, K. Miyazaki, T. Shimada, E. Watanabe, Y. Tateyama, T. Kamiya, T. Honda, J. Akikusa, A. Yamada, *Electrochem. Commun.* **2019**, *104*, 106488.
[26] L. Suo, O. Borodin, W. Sun, X. Fan, C. Yang, F. Wang, T. Gao, Z. Ma, M. Schroeder, A. von Cresce, S.M. Russell, M. Armand, A. Angell, K. Xu, C. Wang, *Angew. Chem. Int. Ed.* **2016**, *55*, 7136.
[27] L. Chen, J. Zhang, Q. Li, J. Vatamanu, X. Ji, T.P. Pollard, C. Cui, S. Hou, J. Chen, C. Yang, L. Ma, M.S. Ding, M. Garaga, S. Greenbaum, H.-S. Lee, O. Borodin, K. Xu, C. Wang, *ACS Energy Lett.* **2020**, *5*, 968.
[28] M.R. Lukatskaya, J.I. Feldblyum, D.G. Mackanic, F. Lissel, D.L. Michels, Y. Cui, Z. Bao, *Energy Environ. Sci.* **2018**, *11*, 2876.
[29] S. Ko, Y. Yamada, A. Yamada, *ACS Appl. Mater. Interfaces* **2019**, acsami.9b13662.
[30] N. Dubouis, P. Lemaire, B. Mirvaux, E. Salager, M. Deschamps, A. Grimaud, *Energy Environ. Sci.* **2018**, *11*, 3491.
[31] M. McEldrew, Z.A.H. Goodwin, A.A. Kornyshev, M.Z. Bazant, *J. Phys. Chem. Lett.* **2018**, *9*, 5840.
[32] L. Coustan, G. Shul, D. Bélanger, *Electrochem. Commun.* **2017**, *77*, 89.
[33] L. Coustan, K. Zaghib, D. Bélanger, *J. Power Sources* **2018**, *399*, 299.
[34] R.-S. Kühnel, D. Reber, A. Remhof, R. Figi, D. Bleiner, C. Battaglia, *Chem. Commun.* **2016**, *52*, 10435.
[35] R.-S. Kühnel, D. Reber, C. Battaglia, *J. Electrochem. Soc.* **2020**, *167*, 070544.
[36] N. Takenaka, T. Inagaki, T. Shimada, Y. Yamada, M. Nagaoka, A. Yamada, *J. Chem. Phys.* **2020**, *152*, 124706.
[37] H. Wang, K. Huang, Y. Zeng, S. Yang, L. Chen, *Electrochimica Acta* **2007**, *52*, 3280.
[38] F. Sauvage, L. Laffont, J.-M. Tarascon, E. Baudrin, *J. Power Sources* **2008**, *175*, 495.
[39] J.-Y. Luo, W.-J. Cui, P. He, Y.-Y. Xia, *Nat. Chem.* **2010**, *2*, 760.
[40] R. Bouchal, Z. Li, C. Bongu, F. Favier, S.A. Freunberger, M. Salanne, O. Fontaine, *Angew. Chem. Int. Ed.* **2020**, *59*, 6.
[41] L. Suo, F. Han, X. Fan, H. Liu, K. Xu, C. Wang, *J. Mater. Chem. A* **2016**, *4*, 6639.

[42] W.T. Hong, M. Risch, K.A. Stoerzinger, A. Grimaud, J. Suntivich, Y. Shao-Horn, *Energy Environ. Sci.* **2015**, *8*, 1404.
[43] M. Kunduraci, R.N. Mutlu, A.M. Gizir, *Ionics* **2020**.
[44] C. Yang, G. Rousse, K. Louise Svane, P.E. Pearce, A.M. Abakumov, M. Deschamps, G. Cibin, A.V. Chadwick, D.A. Dalla Corte, H. Anton Hansen, T. Vegge, J.-M. Tarascon, A. Grimaud, *Nat. Commun.* **2020**, *11*, 1378.
[45] N. Laszczynski, S. Solchenbach, H.A. Gasteiger, B.L. Lucht, *J. Electrochem. Soc.* **2019**, *166*, A1853.
[46] D.J. Xiong, L.D. Ellis, J. Li, H. Li, T. Hynes, J.P. Allen, J. Xia, D.S. Hall, I.G. Hill, J.R. Dahn, *J. Electrochem. Soc.* **2017**, *164*, A3025.
[47] R. Jung, M. Metzger, F. Maglia, C. Stinner, H.A. Gasteiger, *J. Electrochem. Soc.* **2017**, *164*, A1361.
[48] J. Zheng, J. Xiao, W. Xu, X. Chen, M. Gu, X. Li, J.-G. Zhang, *J. Power Sources* **2013**, *227*, 211.
[49] A. Gambou-Bosca, D. Bélanger, *J. Mater. Chem. A* **2014**, *2*, 6463.
[50] J. Betz, G. Bieker, P. Meister, T. Placke, M. Winter, R. Schmuch, *Adv. Energy Mater.* **2019**, *9*, 1803170.
[51] T. Reddy, D. Linden, *Linden's Handbook of Batteries (4th Edition).*, McGraw-Hill Professional Publishing, New York, USA **2010**.
[52] F. Lepoivre, A. Grimaud, D. Larcher, J.-M. Tarascon, *J. Electrochem. Soc.* **2016**, *163*, A923.
[53] W. Yin, S. Mariyappan, A. Grimaud, J.M. Tarascon, *J. Electrochem. Soc.* **2018**, *165*, A3326.

Figure 1. (a) Electrochemical stability window of current collectors and reversibility of Li^+ intercalation/de-intercalation of electrode materials. Cyclic voltammograms performed at 100mV s^{-1} on stainless steel (grey dash line) or Titanium (grey full line) as working electrode (WE), Pt wire as counter electrode (CE) and Ag/AgCl as reference. Cyclic voltammograms performed at 1mV s^{-1} on Mo_6S_8 (dark blue), $LiFePO_4$ (light blue), $LiTi_2(PO_4)_3$ (yellow) $LiNi_{0.6}Mn_{0.2}Co_{0.2}O_2$ (orange) as WE, YP50 activated carbon as CE and Ag/AgCl as reference electrode. (b) Galvanostatic charge and discharge signatures for electrode materials. Galvanostatic experiment performed at 1C on Mo_6S_8 measured in LP30 versus Li metal and 20m LiTFSI versus LFP on SS current collector (1^{st} cycle). Galvanostatic experiment performed at 0.10C on $LiNi_{0.6}Mn_{0.2}Co_{0.2}O_2$ measured in LP30 versus Li metal and 20mLITFSI versus LTP on Ti current collector (1^{st} cycle). All experiments were performed at room t=emperature. 7

Figure 2. Effect of concentration and C-rate on Mo_6S_8/$LiFePO_4$ full cell in LiTFSI based aqueous electrolytes. (a) Capacities of charge and discharge and (b) Coulombic efficiency as a function of cycle number for several concentrations: 5m LiTFSI (brown square), 10m LiTFSI (purple square), 20m LiTFSI (yellow square). Constant current measurements were performed at 1C at room temperature. (c) Capacity of discharge and (d) Coulombic efficiency as function of cycle number for several C-rate: 0.15C, 0.25C, 0.5C, 1C, 2C, 4.5C. Constant current measurements were performed in 20m LiTFSI electrolyte at room temperature. 8

Figure 3. Gas monitoring of Mo_6S_8/$LiFePO_4$ full cell in 20m LiTFSI. (a) Potential and pressure as a function of time at 0.10C monitored in a pressure cell. (b) Potential and hydrogen evolution as function of time at 0.15C monitored using OEMS cell. (c) Amount of gas released per cycle as function of irreversible capacity (dash line is a guide to the eyes). 11

Figure 4. Electrochemical storage of Mo_6S_8/$LiFePO_4$ in 20m LiTFSI. (a) OCV decay measured for a fully charged cell during rest. (b) Time needed to end the 2^{nd} insertion plateau during the resting period as function of the time spent to form SEI during charge. 13

Figure 5. Assessment of the SEI stability over time by mimicking its formation on inert material in 20m LiTFSI electrolyte. (a) Cyclic voltammetry performed at 50mV s^{-1} in a 3-electrodes cell using glassy carbon as working electrode, Pt wire as counter electrode and silver wire as pseudo-reference. The first (red) and the fifteenth (green) voltammograms are shown, as well as the one recorded and after 1 hour OCV. (b) Illustration of the SEI formation and its partial dissolution after a resting period of 1h. 14

Figure 6. Practical consequences of temperature and self-discharge tests on the life of a Mo_6S_8/$LiFePo_4$ cell in 20m LiTFSI. (a) Charge and discharge capacities as a function of cycle number at 55°C for several C-rates. (b) Comparison between charge and discharge capacities and Coulombic efficiency as a function of cycle number for cells cycled at 0.5C at 25°C (yellow) and 55°C (pink). (c) Potential as a function of time for cells cycled at 0.5C at 25°C and 0.5C at 55°C showing the shift of the HER plateau shift depending on the temperature. (d) Potential as a function of time for 3 cells cycled in same conditions, at 0.5C and 55°C, showing the poor reproducibility of cell performances at elevated temperature. (e) Charge and discharge capacities as a function of cycle number for 3 cells cycled at 0.5C at 55°C and range of values for 3 cells cycled at 0.5C and 25°C. (f) Potential as a function of time at 1C during the charge/storage protocol. (g) Coulombic efficiency and discharge capacity as function of cycle number for a cell undergoing charge/storage protocol (green) and continuous cycling (brown) at 1C. 16

Figure 7. Gas monitoring and practical performances for a Mo_6S_8/LFP battery using 20m LiTFSI and 8m LiBETI superconcentrated aqueous electrolyte. (a) Potential and pressure as function of time at 0.10C monitored using a pressure cell. (b) Potential and hydrogen evolution as function of time at

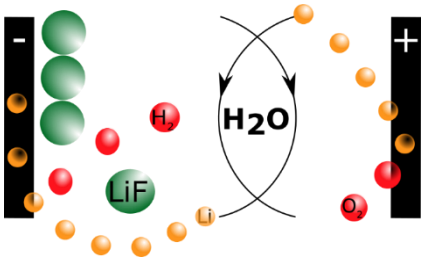
0.10C monitored using an OEMS cell. (c) Cyclic voltammetry performed at 35°C at 50mV s^{-1} in a 3-electrodes cell using glassy carbon as working electrode, Pt wire as counter electrode and saturated calomel electrode as reference. The first (red) and the fifteenth (green) voltammograms are shown, as well as the one recorded and after 1 hour OCV. (d) Coulombic efficiency and discharge capacity as a function of cycle number for a cell undergoing charge/storage protocol (green) and continuous cycling (brown)) at 1C (values are the average calculated with 3 cells). (e) Comparison between charge and discharge capacities and Coulombic efficiency as a function of cycle number for cells cycled at 0.15C at 25°C (yellow) and 55°C (pink). 20

Figure 8. Potential and pressure measured as a function of time for NMC_{622}/LTP cells cycled in (a) Water-in-salt 20 m LiTFSI electrolyte at 25°C, (b) at 55°C (note that the peak observed below 80 hours for the pressure is due to an opening of the oven) and (c) Water-in-bisalt 20 m LiTFSI + 8 m LiBETI at 55°C. 24

Figure 9. Benchmarking WiSE-based and WiBS-based aqueous batteries against other aqueous systems, namely Pb-acid, Ni-Cd and Ni metal hydrides (Ni-MH) batteries as well as against aprotic Li-ion batteries. The spider-chart at the center compares these systems in terms of six parameters defining the overall performances of these systems. On top is compared the specific energy for these systems, on the left the self-discharge for these systems, on the right the energy density, on the bottom left is represented the specific energy as a function of specific power,on the bottom right is reported the energy efficiency for these systems while on the bottom the operating temperature window for the different technologies. All references are given in Supporting Informations. 27

TOC

Water-in-salt Electrolyte (WiSE) for Aqueous Batteries: A Long Way to Practicality



Lithium ion batteries based on superconcentrated aqueous electrolyte shows perfomances that are not competitive yet with organic electrolyte based LiB nor with commercial aqueous batteries such as Lead-acid, Ni-Cd or Ni-MH. Poorer performances are attributed to the SEI instability leading to continuous electrolyte consumption during both cycling and storage period.

Copyright WILEY-VCH Verlag GmbH & Co. KGaA, 69469 Weinheim, Germany, 2018.